Final Technical Report
COVER PAGE

Federal Agency to which Report is submitted: DOE EERE – Wind & Water Power Program
Recipient: University of Massachusetts Amherst, DUNS 153926712
Award Number: DE-EE0007032
Project Title: A Biomimetic Ultrasonic Whistle for Use as a Bat Deterrent on Wind Turbines
Project Period: Sep 1, 2015 - Dec 31, 2019
Principle Investigator: Dr. Paul R. Sievert, Research Associate Professor, psievert@eco.umass.edu, 413-545-4888
Report Submitted by: Paul R. Sievert
Date of Report: September 1, 2021

Working Partners:
Dr. Yahya Modarres-Sadeghi, UMass, 413-545-2468, modarres@engin.umass.edu
Dr. Banafsheh Seyedaghazadeh, UMass, 413-545-1027, bseyedag@umass.edu
Dr. Elizabeth R. Dumont, UMass, 413-545-3565, bdumont@bio.umass.edu
Dr. Matthew A. Lackner, UMass, 413-545-4713, lackner@ecs.umass.edu
Daniel Carlson, UMass, 413-545-1027, dwcarlso@umass.edu
Zara Dowling, UMass, 413-588-1618, zdowling@eco.umass.edu
Dr. Michael Smotherman, Texas A&M, 979-845-6504, msmotherman@bio.tamu.edu

Cost-Sharing Partners: Massachusetts Clean Energy Center, 63 Franklin Street, 3rd Floor, Boston, MA 02110
DOE Project Team: DOE HQ Director – Robert Marlay
DOE HQ Program Manager – Jocelyn Brown-Saracino
DOE HQ Technical Manager – Raphael Tisch
DOE Field Contract Officer – Pamela Brodie
DOE Field Grants Management Specialist – Jane Sanders
DOE Field Project Officer – Bradley Ring
DOE Field Project Monitor – Corrin Macluckie

Signature of Submitting Official: 

• *Acknowledgment:* "The information, data, or work presented herein was funded in part by the Office of Energy Efficiency and Renewable Energy (EERE), U.S. Department of Energy, under Award Number DE-EE0007032."

thereof. The views and opinions of authors expressed herein do not necessarily state or reflect those of the United States Government or any agency thereof."

EXECUTIVE SUMMARY

Our project goal was to design a novel mechanical ultrasonic deterrent for use on wind turbines in order to reduce bat fatalities around these structures. Our proposed deterrent design would be composed of a series of ultrasonic pulse generators, or whistles, affixed to a wind turbine blade, which produce ultrasound through mechanical means. The whistles would produce sounds mimicking the spectrotemporal patterns of bat echolocation pulses, thereby enhancing the bats' ability to detect, localize and avoid the moving blades. These whistles are intended to be operated passively, blown by the wind, and to be positioned at intervals along a turbine blade. Because the source of sound generation will be mechanical in nature, these devices will require no external power source, should require little maintenance, and will be small and cost-effective.

Due to rapid attenuation of ultrasound in the atmosphere, hub-mounted high frequency ultrasonic deterrents cannot cover the entire rotor swept zone (RSZ) of a turbine. The small size of our devices will allow us to position them along the turbine blade, ensuring full ultrasonic coverage of the RSZ. These devices should have an insignificant impact on blade efficiency, and we anticipate that these devices could ultimately be housed within vortex generators, which are known to delay flow separation and increase efficiency of turbine blades.

The following objectives guided the development of our ultrasonic deterrents:

1) Derive design parameters for an ultrasonic deterrent based on avoidance responses to sound regimes by at-risk bat species,
2) Design biomimetic model of bat larynx, which reproduces key aspects of ultrasonic behavior, and confirm the prototype whistle acoustic behavior in laboratory and wind tunnel,
3) Model and experiment to derive altered designs which display similar behavior, but at altered frequencies,
4) Evaluate bat avoidance response to sound regimes produced by series of prototype whistles, and
5) Test whistle acoustic behavior on small-scale wind turbine.

To address the objectives above, we structured our research around seven major tasks:

1) Characterize bat avoidance responses to ultrasound regimes
2) Design an initial biomimetic prototype
3) Develop a series of prototype whistles operating over a range of frequencies: 25-35 kHz, 35-45 kHz, and 45-55 kHz ranges
4) Complete research to develop the frequency, intensity, and pattern specifications that leads to deterrence of free-flying bats
5) Test prototype whistles on a wind turbine
6) Define operating variables under which the whistles will need to be able to perform
7) Develop a revised biological study design that incorporates the insights from other researchers in the field and uses only sounds produced from the whistles, rather than generic ultrasonic sounds.

We began to address these tasks by modeling our prototype whistles on the larynx of the greater horseshoe bat (*Rhinolophus ferrumequinum*) and the vocal membranes of the concave-eared torrent frog (*Amolops tormotus*). Our studies showed that we could reduce the complexity of larynx geometry to a tensioned film in flow, and our device could produce ultrasound using flow-induced oscillations in the desired frequency and power range.

Next, we evaluated the effect of ultrasounds from our prototype whistles on flight behavior of Mexican free-tailed bats (*Tadarida brasiliensis*) and tricolored bats (*Perimyotis subflavus*) in the laboratory using a turning assay that quantifies flight changes in response to ultrasound. Flight paths of Mexican free-tailed bats were significantly modified by the ultrasound, while pipistrelles were unaffected. We then attempted to evaluate the effects of our ultrasound deterrents on free-flying bats using thermal imaging cameras but were unsuccessful since bats did not come within 100 m of our playback speakers.

To address Task 6, we built a small-scale wind turbine in order to investigate the performance of our prototype whistles in flow similar to that encountered by a full-scale wind turbine blade. In the course of designating the desired flow velocity to actuate our bat deterrent device, we investigated the flow conditions about a rotating wind turbine blade. The current device performance is primarily dependent on the velocity of the incoming flow, leading us to focus on the nature of flow separation along a turbine blade. For a full-scale turbine blade, the edgewise velocity distribution is of appropriate magnitude for actuation of the bat deterrent. For locations closer to the root or farther downstream on the chord, early results show favorable performance for flow concentrators. However, as actual deployed wind turbine blades have proprietary geometries, full-scale deployment of the deterrent will require close collaboration with the blade manufacturers. Such collaboration would permit the design of flow concentrators custom-built for their specific placement along the length of the blade.

Conclusions and Recommendations for Further Study

We originally used a biomimetic approach to design an ultrasonic whistle that could be passively activated when attached to a wind turbine blade, producing ultrasound that would potentially deter bats from approaching turbines. Later in our study, we found that it was possible to simplify this approach and use a tensioned film in flow to produce ultrasound in the 25-35 kHz, 35-45 kHz, and 45-55 kHz ranges. We then played recordings of these sounds to bats in a laboratory setting, and showed that flight paths of Mexican free-tailed bats were affected, but tricolored bats were not. The next critical steps in this research program are to test the effects of sounds created by ultrasonic whistles on free-flying bats (we attempted to do this, but without success), and if results are promising, to deploy the deterrents on the blades of functioning wind turbines. Passively activated ultrasonic deterrents have great potential for reducing bat mortalities and because they are small and can be deployed along a turbine blade without negatively impacting performance, they may be a very practical solution to conserving bat populations.

List of Figures:

ACCOMPLISHMENTS

Task 1: Characterize bat avoidance responses to ultrasound regimes

> **Deliverable 1** – Complete a report summarizing results from lab trials and detailing the technical operational specifications (frequencies, intensities, and sound patterns) needed for the development of an ultrasonic deterrent device. (Report submitted Sep. 16, 2016)

DELIVERABLE 1: BAT AVOIDANCE RESPONSES TO ULTRASOUND REGIMES

TASK SUMMARYCompletion of the two originally proposed behavioral assays, Y-maze and Perch selection, produced conflicting results. From these experiments we developed a third assay (Turning Assay) that appears better suited to test how the bats will respond to the proposed device in nature. That assay produced reliable evidence that broadband noises can work as acoustic deterrents. Although a continuous broadband (white) noise was somewhat effective, short, broadband clicks overlapping with the lower frequency range of the bats own pulses were statistically more effective. Cumulatively, results indicate that the proposed device can alter bat flight paths when presented in a behaviorally meaningful context, and that the optimal acoustic parameters for different species can be predicted based on known auditory characteristics (i.e., the bats just have to be able to hear it).

THREE BEHAVIORAL ASSAYS

1) Y-Maze – Mexican free-tailed bats were given a choice to fly down either of two sides of a divided tunnel. One side had a continuous acoustic stimulus playing (computer generated) while the other was quiet. We measured the percentage of flights down both sides.

2) Perching – Bats were released into a room with smooth walls and a ceiling. They could not easily perch anywhere except on two feeding platforms at opposite sides of room, making this essentially a two-alternative forced choice assay. Both perches have a speaker. During trials, one of the speakers was ON, and we count how many times the bats land on either perch (stimulus vs quiet perch).

3) Turning – Bats fly down an open tunnel. Their approach triggers a stimulus playback (PB) from either of two speakers positioned on opposite sides of tunnel. We assess whether the PB altered flight paths by recording which direction the bat turned in response to PB (towards or away from PB speaker).

ASSAY 1: Y-MAZE

Sample Size:
- 6 bats, 20 flights per bat

Results:

- There was no statistically significant effect of any stimulus on flight path choice of bats (Chi-square test: P>0.05; Fig. 1).

- The Y-maze assay did not work the way we expected it to for three reasons:
    1) The bats quickly adapted to the stimulus: once they'd mapped out the layout of the room and adapted to the stimulus they ignored it.
    2) The acoustic stimuli were not noxious and were not sufficiently annoying to degrade the bats sonar performance (in other words, the bats heard the different stimuli but were not sufficiently motivated to avoid the sounds).
    3) Each bat showed a high degree of "handedness", or personal preference for going down the left or right sides of the maze. This "handedness" increased the standard deviation, requiring a much larger sample size than anticipated.

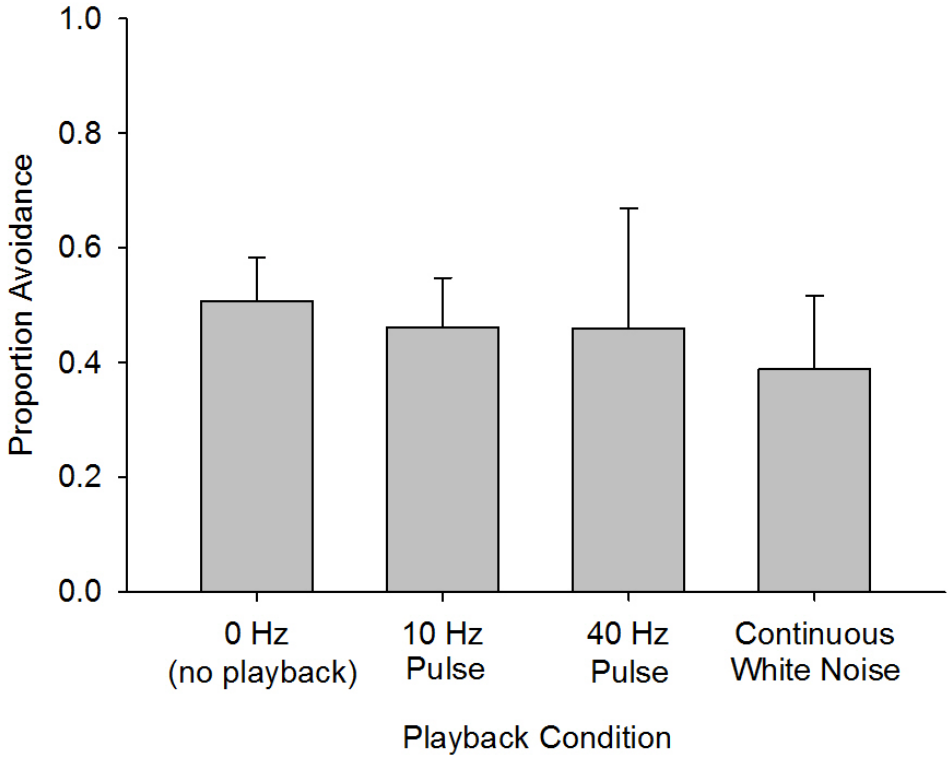

Fig. 1. Avoidance response of Mexican free-tailed bats to acoustic stimuli in a Y-maze testing format.

Conclusions:
This experiment did not work, primarily because the Mexican free-tailed bats quickly adapted to the stimulus and weren't motivated to avoid it. Increasing sample size will not change these results. However, these trials led us to a better experimental design that did work (the Turning Assay).

ASSAY 2: PERCHING

Sample Size:
- 10 Mexican free-tailed bats, >10 landings per trial.

Experiments:
Experiment 1: Bats chose between a quiet perch and a perch with broadband clicks.
Experiment 2: Bats chose between a quiet perch and a perch with continuous white noise.

Results:
- Repeated-measures ANOVA revealed a significant effect ($F_{3,39} = 51.1$, $P < 0.01$). Post-hoc tests show that both CLICKS and continuous NOISE stimuli repelled bats, but CLICKS were significantly more effective than NOISE ($p < 0.001$; Fig. 2).
- In summary, bats avoided perches with noise stimuli in favor of quieter perches. Clicks were more effective than noise. We have yet to try a wider array of stimulus parameters.

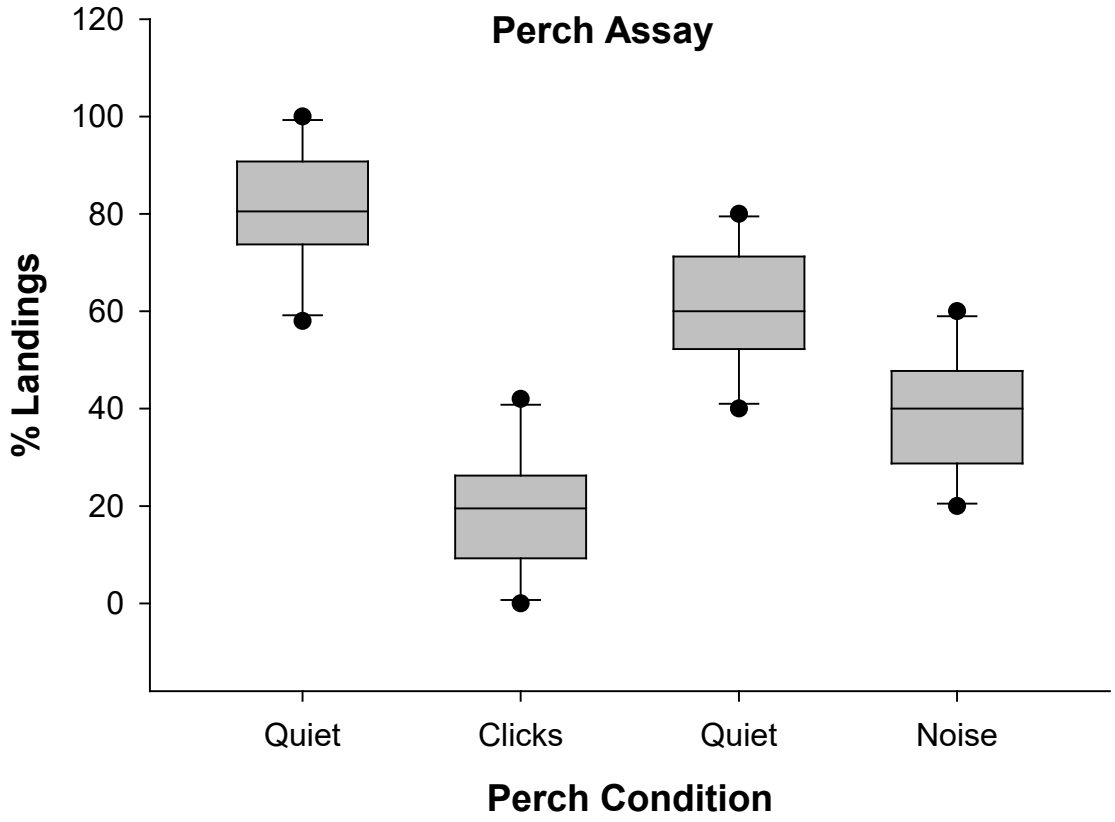

Fig. 2. Landing response of Mexican free-tailed bats to acoustic stimuli as measured in the laboratory using a perch assay.

Conclusions: This experiment worked as expected, and has the added advantage of not requiring trained bats. This may be the easiest assay for testing different acoustic parameters very quickly.

ASSAY 3: TURNING

Sample Size:
- 6 bats (10 flights/bat/condition)

Experiment:
In this assay we tested broadband clicks (10 ms duration, 10 kHz-40 kHz bandwidth), using bats that were trained to fly back and forth between two feeding platforms. For controls, we ran the stimulus program with the speaker OFF. The room is completely dark, but illuminated with IR light (Fig. 3). There is also a small IR LED connected to each speaker: the LED flashes whenever the bat triggers the playback (PB; 10 clicks delivered from the right or left speaker at a rate of 50 clicks per second, thus mimicking the sound of a rapidly approaching obstacle, or bat). The bat does not know if, when, or from which side the PB will be triggered.

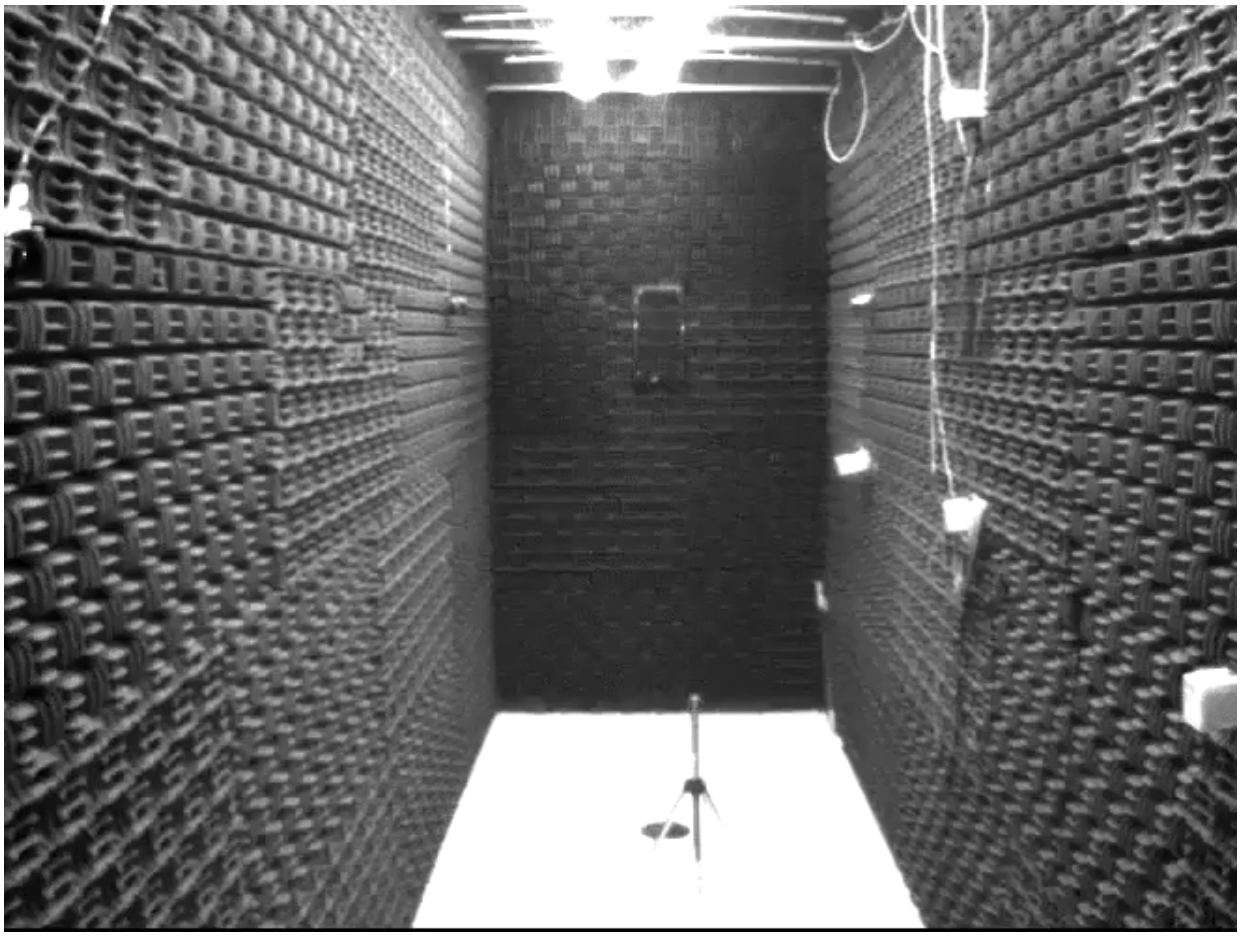

Fig. 3. Testing chamber used in turning assay of response of bats to acoustic stimuli.

Conclusions: Stimulus side was positively correlated with direction of turn $p < 0.001$). This assay works well and seems most appropriate for testing whether the proposed device can alter flight paths in the wild.

Task 2: Design initial biomimetic prototype

> **Deliverable 2** – Complete a report identifying one or more candidate biological models, and the three-dimensional numerical models of these systems appropriate for analysis in OpenFoam. (Report submitted Mar. 8, 2016)

DELIVERABLE 2: IDENTIFICATION OF CANDIDATE BIOLOGICAL MODELS FOR ULTRASOUND PRODUCTION

TASK SUMMARY

As part of the design process for our bat deterrent device, we examined existing models of ultrasonic frequency (>20 kHz) sound production. Our primary focus was on the vertebrate larynx (or syrinx in birds), wherein oscillation of the vocal folds is induced by air flow across these flexible structures, without direct muscular control. This system presents a useful model for a deterrent device which is operated mechanically, wherein oscillation and associated sound production will be induced only by air flow across the device, rather than through an independent power source. In this report, we review the basic anatomy of the vertebrate larynx, and briefly cover the types of models that have been developed to date in order to describe and understand these systems. We then consider what is known about high frequency and ultrasonic frequency sound production in nature. We conclude this section with a summary of how these findings pertain to the development of a biomimetic ultrasonic device.

In a second section, we explore aspects of several rigid whistle designs that are commercially available. Among these, dog and deer whistles are purported to produce sound within the ultrasonic range. We highlight unknown variables in these systems, and note issues which may be relevant to design of our deterrent device.

THE VERTEBRATE LARYNX

Basic Anatomy

Mammals, reptiles, and amphibians produce sound in the larynx, an expanded structure at the top of the trachea, supported by cartilage and muscular tissue (Harrison 1995). During phonation (i.e., sound production), air enters the structure via the trachea from the lungs, and exits via the pharynx, that is, the cavity which connects to the nose and mouth. Within the larynx, the vocal folds, also known as vocal chords, are primary structures involved in the production of sound. At their outer edges, these structures are attached to muscles in the larynx, while the inner edges are free to oscillate (Fitch 2006). These “true” vocal folds are protected by “false” vocal folds, or vestibular folds – thick folds of mucous membrane that project above the true vocal folds within the larynx, but do not appear to contribute significantly to sound production. The term “glottis” is often used to refer to the true vocal folds and the slit-like opening that runs between them. Hereafter, “vocal folds” will be used to refer to the true vocal folds.

In simple terms, the oscillations of the vocal folds modulate airflow through the larynx, creating fluctuations in flow which can be perceived as sound (Fitch 2006). The basic rate of oscillation

determines the frequency of the perceived sound. This basic rate, and hence the fundamental frequency of perceived sound, is dependent upon the driving lung pressure and the anatomy of the vocal folds, including size, length, and mechanical properties (Titze 1988). The tension exerted on the vocal folds is under active muscular control, and can be adjusted to produce differing frequencies (Fitch 2006). It is important to emphasize that the oscillations of the vocal folds are not *driven* by muscular movements, however. It is the airflow itself that induces the oscillation, much in the same way that a flag flaps in the breeze. It is the wind that causes a flag to wave, not active whipping of the flag by a motor or other device at the flag pole. To continue this analogy, the size, shape, and material properties of the flag, as well as the wind speed and direction, will affect the movements of the flag, and any sounds produced

The anatomy of the vocal folds has best been described for humans and large mammals. In these species, vocal folds generally consist of at least two layers: a relatively loose 'cover' layer, of epithelial tissue, and a muscular 'body' layer (Hirano and Kakita 1985). Human vocal folds, and those of some other species, have a ligament between the cover and body layers, composed primarily of lamina propria tissue, but the anatomy is not well described in many species. Most of the vocal fold vibrations occur in the cover layer because of its high elasticity and proximity to the driving force of air exiting the lungs (Titze 1988).

Each tissue layer (cover, ligament and muscle) may have differing mechanical properties. One property of great importance is longitudinal elasticity. This property is often described using Young's modulus. Young's modulus is a value derived from tests in which a tissue fiber direction is specified and stress–strain tests are performed along a single dimension, measuring the relationship between applied force per unit area and resulting elastic deformation. In large mammals, including humans, Young's modulus for vocal fold tissue falls in the range of ~20-40 kPa (Alipour et al. 2011), which indicates a high degree of elasticity.

Vocal folds can be variably stretched, in order to produce differing fundamental frequencies (e.g. Hollien 1960, Monsen et al. 1978). As a result, each tissue part reacts with a different tension (Hirano 1974, Story & Titze 1995). The tension of the cover and vocal ligament are controlled solely by vocal fold length, which are in turn governed by muscles attached to cartilage around the larynx. The body, however, has active contractile properties, so that tension is also regulated by active stiffening of the thyroarytenoid muscle. In humans, the vocal ligament has the highest stress-bearing capability, and hence is thought to bear the greatest tension during high-frequency sound production (Titze & Hunter 2004).

Existing Models of the Vertebrate Larynx

The human larynx has been a great focus of scientific attention, with most researchers ultimately interested in treating human pathologies and phonation disorders. The larynxes of other species have received significantly less consideration. A number of models have been used to describe the human larynx.

At the simplest level, the ideal string equation describes the vocal fold as a string, not unlike the string on a guitar. The fundamental frequency corresponding to such a model can be calculated as follows:

$$F_0 = \frac{1}{2L}\sqrt{\frac{\sigma}{\rho}}$$

where
F_0 = fundamental frequency of the oscillation
L = vocal fold length
σ = stress applied to the vocal fold (force per unit area)
ρ = tissue density

Based on this equation, it is apparent that with other properties held constant, the shorter the vocal fold, the higher the fundamental frequency of sound produced. In the mammalian larynx, contractions of the cricothyroid and thyroarytenoid muscles place tension on the vocal fold and can alter the stress exerted, changing the frequency of sound produced (Harrison 1995, Fitch 2006).

Much more complex mathematical and mechanical models have been developed. An early development, the early myoelastic-aerodynamic theory of vocal fold oscillation, has been expanded upon to generate one-mass, two-mass, three-mass, and even up to sixteen-mass models (Cveticanin 2012). A biomechanical model integrating tissue mechanical response with a structural model of beam vibration has been used to predict fundamental frequencies of response (Zhang et al. 2009).

In addition to theoretical models, synthetic models of the human vocal folds have been developed, often using a layered system of silicone (e.g. Murray and Thomson 2012). These models have been made to reproduce important aspects of vocal fold behavior, including mucosal wave-like motion, realistic threshold pressure and frequency (Murray and Thomson 2012). One recent area of study has been in the development of synthetic vocal fold models which exhibit nonlinear material properties (Shaw et al. 2012). These models have been shown to demonstrate a more realistic frequency response to increasing vocal fold length.

High Frequency Sound and Body Size

In development of an ultrasonic device, we are particularly interested in biological models which produce sound at frequencies near or at ultrasonic levels. Simple string theory suggests that an increase in the fundamental frequency of sound produced can be accomplished either by a decrease in length of the vocal fold, a decrease in tissue density, or an increase in stress. An increase in stress requires an associated increase in the ability of the vocal fold to endure that stress.

Observational data demonstrates that one avenue leading to production of ultrasound among mammalian species is indeed a decrease is physical size and length of the vocal folds. Small rodents and echolocating bats are among the few mammals known to produce ultrasonic calls, and there is a general relationship between body size and the frequency of sound produced by mammals (Suthers & Fattu 1973, Finch 2006). We know very little about the material properties of the laryngeal tissue of small mammals, but an examination of the laryngeal anatomy of rats

demonstrated that, for this small mammal at least, vocal fold tissue behaves similarly under stress-strain tests to larger, better-studied mammal species (Riede et al. 2011). Calculations using the ideal string equation suggest that the short vocal fold of the rat should be able to oscillate at rates up to ~6 kHz. This overlaps well with known vocalizations in the range of 1-6 kHz for rats (Riede et al. 2011). Rats are also known to produce ultrasound (>20 kHz), but via a separate, whistle-like mechanism, which has not been well-described (Roberts 1975a,b).

A revealing exception to the body size-frequency relationship is the case of the Rocky Mountain elk (*Cervus elaphus nelsoni*), which during the fall mating season produces high frequency sound in the range of ~1 kHz, using a vocal fold of approximately 3 cm (Riede and Titze 2008). Based on ideal string theory, it was hypothesized that this species must have evolved a highly elastic vocal ligament in order to sustain the tension necessary to generate such frequencies. Simple calculations suggest that to produce high frequencies on a vocal fold of that length, the vocal ligament would have to withstand tensions approximately an order of magnitude (9x) higher than those known in the most stressed human vocal cords. Testing of the elk vocal ligament, however, revealed elastic properties were similar to those found in human vocal fold tissue. Rather than possessing highly elastic properties, it is thought that the elk must have adaptations that reduce the effective size of the vocal fold, either due to bending properties along the vocal fold, or movement of the boundary associated with active muscle stiffening (Riede and Titze 2008).

Bats as Models of Ultrasound Production

Bats are, of course, one of the few taxa of vertebrates that produce calls at ultrasonic frequencies (> 20 kHz). While part of their ability to produce such calls is likely due to their small size, other aspects of their laryngeal anatomy may also play a role in ultrasound production. Vespertilionids, and other bat species, have vocal folds which terminate in very thin membranes known as vocal membranes (Suthers and Fattu 1973). These structures are found primarily in echolocating bats and non-human primates, although they have been observed in some small felids, llamas, and young pigs (Mergell et al. 1998). The membranes are formed of connective tissue and lack muscle fibers. In bats, they can be as thin as a few microns across (Suthers and Fattu 1973). Researchers have put forward a number of theories regarding the purpose of these structures (Mergell et al. 1998). It has been suggested that the stiff, lightweight membranes could vibrate relatively independently of the rest of the vocal folds, allowing for the production of extremely high frequency calls, and hence providing a wider pitch range. Alternatively, it has been suggested that membranes could result in greater vocal efficiency through a decrease in the threshold pressure required for sound production. A final theory is that vocal membranes lead to the production of chaotic vibration (Mergell et al. 1998).

Simulations using simple models of larynx behavior suggest that vocal membranes may permit the vocal folds to oscillate at lower subglottal threshold pressures, and indicate that this effect increases with increasing frequency (Lucero 1995). The presence of vocal membranes may allow mammalian vocal folds not only to produce higher pitched phonation, but also to do so more loudly and efficiently. Simulations further suggest that there is an optimal angle of attachment for any given membrane length to lower threshold pressure. Although no data exists to test this conjecture, it has been hypothesized that the membranes can vary in their angle of attachment to

the vocal fold during sound production, acting as an independent oscillator. It has also been suggested that the addition of vocal membranes makes sound production more susceptible to any vocal fold asymmetry, and thus more likely to enter regimes of subharmonic or chaotic vibration (Mergell et al. 1998). This theory is supported by an examination of the vocal folds of a wolf hybrid which displayed aberrant nonlinear sound production during howling (Riede et al. 2000). The vocal folds of this animal had finger-like extensions similar to vocal membranes, which were not found on other individuals of the same family.

Vocal membranes aside, the structure of the bat larynx is similar to that of humans and other mammalian systems. As in other species, the tension in the vocal folds and membranes controls their oscillation frequency within the range set by the anatomy of the vocal folds. The tension is adjusted by rotation of the thyroid cartilage around the cricothyroid joint, and mainly controlled by the bat's cricothyroid muscle (Fig. 4; Elemans et al. 2011). In bats that produce frequency-modulated calls, the vocal folds are tensed prior to sound production (Suthers and Fattu 1973). As the cricothyroid muscle contracts to tense the vocal folds, the glottis closes (Durrant 1988). As the crichothyriod muscle relaxes, the glottis open and the vocal folds relax, allowing air to flow across the vocal folds and produce a downward frequency-modulated call (Suthers and Fattu 1973).

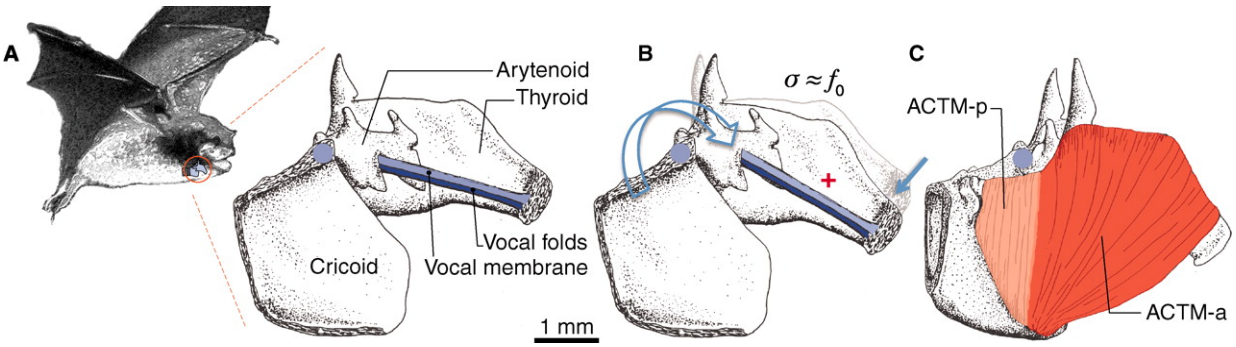

Fig. 4. Sound frequency modulation during echolocation calls [from Elemans et al. 2011]. (**A**) Proposed frequency control mechanism of echolocation calls illustrated in schematic representation of a vespertilionid bat larynx [adapted with permission from R. A. Suthers]. Flow-induced self-sustained oscillations of the vocal folds (dark blue) and vocal membranes (light blue) generate ultrasonic pressure fluctuations. Their tension (σ) determines the fundamental frequency (f_0) of self-sustained oscillations. (**B**) Rotation (blue arrows) of the thyroid cartilage around the cricothyroid joint (blue circle) causes the vocal folds and membranes to stretch and adduct while the arytenoid cartilage remains stationary (*7*). This rotation increases fold and membrane length and tension (red plus) and thereby increases the fundamental frequency of produced sound. (**C**) The anterior cricothyroid muscle (ACTM) controls cricothyroid rotation and consists of an anterior (ACTM-a) and posterior part (ACTM-p). Relaxation of the ACTM-a results in f_0 decrease during phonation.

The excised larynx of the greater horseshoe bat (*Rhinolophus ferrumequinum*) provides a particularly relevant model for a mechanical whistle device. Not only does this anatomical structure consistently produce ultrasound, but it will exhibit nonlinear sound production in response to small changes in air flow (Kobayasi et al. 2012). Between air pressures of 1.5-3 kPa, the sound intensity of the fundamental frequency of the larynx rises and then decreases with increasing air pressure, but remains fairly high throughout (63-82 dB Sound Pressure Level -

SPL). At the low end of this air pressure range, the fundamental frequency begins at or around 32.5 kHz, climbing with increasing pressure to ~35 kHz. The bat larynx then demonstrates a dramatic frequency jump, with the fundamental frequency dropping ~13 kHz, to around 21-23 kHz. This frequency jump occurs across a pressure change of less than 0.05 kPa. From this lower frequency, the fundamental frequency again begins to slowly rise. Increasing air pressure above ~3 kPa leads to aperiodic chaotic emission of signals with bandwidths greater than 10 kHz. Importantly, Kobayasi et al. (2012) found that the acoustic properties of the bat's sonar pulses emerged solely from the mechanical properties of the larynx. This supports the idea that nonlinear sound can be generated by a purely mechanical device provided with the appropriate air pressure gradient.

The Concave Eared Torrent Frog as a Model of Ultrasound Production

A second model of interest in the generation of nonlinear ultrasound is that of the concave-eared torrent frog (*Amolops tormotus*). Males of the species produce a variety of warbling calls that extend well into the ultrasonic range. Nonlinear acoustic phenomena include period doubling, frequency jumps, and chaos (Suthers et al. 2006). These phenomena can be reproduced by blowing air through the excised larynx of a euthanized frog specimen. The frog has T-shaped vocal folds, and it is thought that the ultrasound is most likely produced by oscillation of the cranial portion of the medial vocal ligament within these vocal folds.

Relevance to Device Design

The anatomy of the human larynx has been well studied and modeled, both mathematically and physically using synthetic models composed of flexible materials. The challenge for our team is that the structures within the larynxes of organisms that produce ultrasound have not been described in great detail, and the processes through which these structures generate non-linear acoustic patterns are not well understood. It does appear that oscillation of thin membranes (the vocal membranes of bats or T-shaped vocal chords of concave-eared torrent frogs) is important for ultrasound production, and likely relevant to the production of non-linear acoustic phenomena. These structures will therefore be one area of focus for our team.

The material properties of laryngeal tissue in ultrasound-generating organisms also have not been measured. From what research has been done, it appears that material properties, or at the very least the elasticity of laryngeal tissue, is conserved across a variety of mammalian species (e.g. human, elk, rat). We therefore proceed from the assumption that the laryngeal tissue of echolocating bats and the concave-eared torrent frog is similarly elastic, with a Young's modulus of the same order of magnitude of these taxa (~30 kPa). This value for Young's modulus indicates that the material used to produce these synthetic structures must be highly elastic, necessitating the use of silicone or similar materials in our biomimetic devices. In addition, the damping coefficient of the material must be sufficiently small, as viscous damping manifests as a per-cycle reduction in the amplitude of oscillation, which means high frequency signals are more quickly attenuated over time. Current three-dimensional printing technology can incorporate flexible materials, but these materials have high damping, and are therefore not appropriate for synthetic models. We must instead rely on casting silicone and other flexible materials in molds constructed using three-dimensional printing.

It is apparent, also, that the short length of vocal folds of ultrasound-emitting species play a large role in determining the high frequencies they generate. For manufacturing purposes, we will likely find it necessary to create devices that are significantly larger than our biological models. Initially, we therefore expect oscillatory frequencies to be significantly lower than those seen in nature. Eventually, we should be able to address this issue through one of several means. As with the elk, we may be able to create effectively smaller structures by creating boundaries along a larger flexible element. Alternatively, we may be able to find a manufactured material that can withstand greater tension without breakage, and that meanwhile does not quickly damp oscillations. Given the complexities involved in computationally modelling oscillations of flexible systems, we expect to begin with an experimental approach, creating synthetic models of relevant systems (concave-eared torrent frog, bats) using techniques designed for human larynx models. Our theoretical understanding of these systems will be informed by computer models of rigid versions of these systems.

ULTRASONIC WHISTLE DESIGNS

Whistles are a relatively simple mechanism for sound production, and there exist a variety of types designed for widely varying applications. In most cases, these devices are not ideal models in that they are typically not designed to operate in the ultrasonic range, since it is usually not useful to have a whistle which operates outside the hearing range of humans. Exceptions include a special class of ultrasonic Galton whistles, used for communication and training of dogs, and a second group of devices designed as vehicle-mounted ultrasonic deterrents for deer. Hutchins et al. (1983) also designed a series of ultrasonic whistles producing predictable high intensity sound (>100 dB) across a range of frequencies (16-160 kHz). However, these whistles required high-pressure inputs of ~350 kPa, which are unlikely to be produced or induced on turbine blades, and we therefore do not give them further consideration here.

Dog Whistles

The original Galton whistle was developed by Sir Francis Galton in 1883 to test the hearing ability of human subjects. Galton used these whistles to further test the ability of various animal species to hear high frequency sound. These devices were eventually adapted for use as dog whistles, allowing communication between a trainer and a dog above the range of human hearing. Modern, mass-produced dog whistles are typically rigid metal or plastic, and composed of two parts, an outer casing which includes a mouthpiece, and a smaller screwing component, which allows adjustment of the size of the sound chamber in order to adjust frequency (Topman et al. 2004). Air is blown by a person through a mouthpiece, with the jet of air striking a sharp edge or “splitter.” Oscillation of the air alternately above and below this sharp edge leads to the generation of standing waves within the air column beyond the sharp edge. The fundamental frequency of the air column, and sound produced, is primarily dependent on the length and diameter of the air column (Chanaud 1970).

Dog whistles are often described as “silent” or “ultrasonic,” but manufacturers rarely list the frequencies produced, and when they do, frequencies are typically not in the ultrasonic range. For example, Gun Dog Suppliers describes the Acme Silent Dog Whistle as active in the 5-12.4

kHz range, which is below the maximum human range of hearing of ~20 kHz. There is very little test data available on the range of frequencies actually produced by dog whistles, the volume or intensity of sounds produced, or the air pressure thresholds required to generate sound. One early paper (Pattie 1924) describes the development of a continuous blower for a Galton whistle, operating at a constant air pressure of 1 kPa. Others describe tests using input pressures of 0.5 kPa-2.5 kPa (Scripture & Smith 1894), but output sound intensity is not reported.

Deer Whistles

Of all man-made ultrasonic devices, deer whistles are perhaps the most similar in concept to a bat deterrent device. These inexpensive plastic whistles are intended to be attached to the front bumper of a car or truck. As the vehicle is being driven (typically advertised for speeds exceeding 30 mph), wind generated by this motion drives air against a sharp edge, generating sound described as ultrasonic. The sound is supposed to warn deer of approaching vehicles, and avoid deer-vehicle collisions. Schefiele et al. (2003) found closed and open-ended versions of these devices actually operated well below ultrasonic frequencies. Closed-end whistles generated sound in the range of ~3.3 kHz, with little change in frequency as air pressure changed (±0.13 kHz). Open-end whistles operated at a frequency of ~12 kHz, with greater changes associated with changes in air flow (±1.23). The loudest closed-end whistles had a sound intensity of 70 dB at 20 uPa, the open-end varieties of 36 dB at 20 uPa. While in wide use across the country, there is little evidence that these devices are effective; one review study termed them “useless” (Hedlund et al. 2004).

Varying Tones in Whistles

The fact that whistles often produce a single tone is of concern, since this type of sound is not thought to effectively deter bats. The police whistle is one exception to this pattern, producing a warbling pattern varying in frequency (Chanaud 1970). This whistle operates via a similar principle to the aforementioned whistles. Sound is produced when air is blown through a mouthpiece and creates an edge tone in the slot at the top. A cylindrical air cavity contains a balls which rotates through the cavity. The rotating ball periodically blocks the hole and stops the tone, generating variety in the sound produced (Chanaud 1970).

Relevance to Device Design

Our review suggests there is very little information in the published or gray literature regarding performance of dog whistles, in terms of threshold air pressure required to generate sound, output frequency, and output sound intensity. Manufacturers often claim whistles are “ultrasonic,” but it is not clear that these devices actually perform within this range (>20 kHz). A number of very old papers suggest Galton whistles can be operated at fairly low air pressures, but output sound intensities are not reported. Similarly, we found only one published study documenting frequencies of sound produced by deer whistles. This study found frequencies were below the ultrasonic range, though advertised as ultrasonic. Output intensities were somewhat high for closed-end whistles, but not likely to exceed ambient noise over long distances. Deer whistles produced sound when vehicles were driven at speeds exceeding 40 mph (17 m/s), but input air pressure was not reported, nor the minimum speed required to generate sound. In sum,

dog and deer whistles are in concept good models for ultrasonic whistle design, but may not be useful models in practice. In order to determine whether these devices could provide suitable models for our device, we would need to conduct trials of a variety of these whistles in the laboratory under controlled conditions.

From our perspective, most whistle designs suffer from the problem of generating a fairly consistent frequency across air pressure inputs. In order to use a rigid whistle design, we would need to incorporate some type of interrupter device, such as the kind employed in the policeman's whistle.

Deliverable 3 – Complete a report that provides theoretical estimates of frequency and amplitude output for the candidate model(s). (Report submitted Mar. 8, 2016)

DELIVERABLE 3: DIGITIZED AND PHYSICAL MODELS FOR ULTRASOUND PRODUCTION

TASK SUMMARY

During the first quarter of the project our technical efforts centered on modeling laryngeal anatomy both computationally and physically, with the goal of determining which structures play roles in producing ultrasonic sounds. We conducted experiments using a rigid dog whistle, made progress toward development of a 3-dimensional bat larynx model, and used a torrent frog larynx model for both design and experimental work. The torrent frog model has been shown to produce patterns of ultrasonic sound of interest, and is better understood than the larynxes of representative bat species. Mid-portion and dorsal-third sections of the vocal cords of the concave-eared torrent frog were digitized and the mid-portion was revolved to develop a simple, axially-symmetrical model of the larynx. This simplified model was used for computational fluid dynamics modeling using ANSYS Fluent and OpenFOAM software. We also developed methods to accurately manufacture scaled versions of this model out of flexible materials, using a molding process that will be useful in future stages of the project. The prototype larynx model was tested using a pressurized air-line and in the UMass wind tunnel. Flow visualization at an applicable Reynolds number revealed flow stagnation upstream of the larynx, indicating a need to develop flow concentrators to increase air flow through the device. We also suspect that flow stagnation was an issue with the dog whistle we tested initially.

INTRODUCTION

We have used computational and experimental approaches to focus on two models for ultrasonic sound production: rigid and flexible structures. Rigid devices, such as dog whistles and deer whistles, have the advantage of being inexpensive, easy to manufacture, commercially-available, and advertised to operate in the desired ultrasonic range. The downside of these whistles is that the input threshold for air flow may not be realistic for wind turbine applications, the output intensities are unknown, and it is possible that they may not produce the necessary ultrasonic

frequencies. Perhaps most importantly, these whistles produce only a single tone across a range of input air flows, and therefore may not be a successful deterrent for bats. Initially, we conducted experimental work on a dog whistle, but recently we have focused on flexible structures based on the vertebrate larynx model. The advantage of the vertebrate larynx system is that we know excised larynxes can produce high intensity ultrasound with relatively low input pressure, and that nonlinear frequency changes can occur as the result of small changes in input air pressure. We believe that this dynamic system is the most likely to produce ultrasounds that can act as deterrents to bats.

DOG WHISTLE TESTING

Initially, we tested a dog whistle using a pressurized air-line in the Fluid-Structure Interactions Laboratory at the University of Massachusetts Amherst, and then in the UMass wind tunnel facility.

In dog whistle-style devices, a jet of air is blown across a hole in the side of the whistle, and this jet impinges on a sharp edge, thus creating an edge tone. The tone makes the column of air in the cavity beyond the hole resonate at a specific frequency. The characteristics of the emitted sound are determined by the length and diameter of the cavity, as well as the geometry of the sharp edge (Fig. 5).

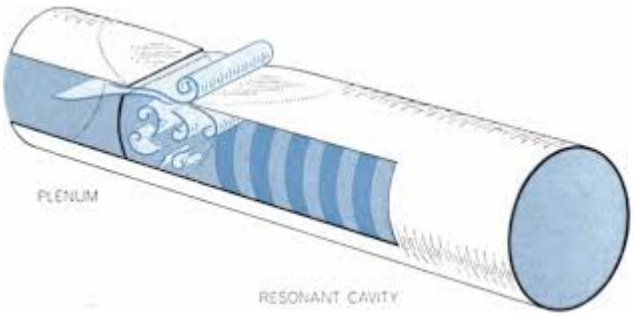

Fig. 5. Schematic of air flow through a dog whistle (Chanaud 1970).

In our initial laboratory experiment we connected a pressurized air-line to the inlet of a dog whistle, and placed an AR125 ultrasonic receiver 2 cm downstream of the whistle outlet. The receiver can capture frequencies up to 125 kHz, and has a 90 dB dynamic range. Figure 6 shows a sample spectral response of the sound emitted from the whistle under an input pressure of 18 PSI. Three distinct peaks at frequencies of f=18, 54, and 90 kHz were observed, where the frequency response consisted of the main harmonic (f_1=18 kHz), and the higher harmonics acting at three and five times the fundamental frequency. The amplitudes of the recorded sounds were 90, 80, and 70 dB, respectively. We were encouraged to observe that the existing design produces high intensity sound at a high frequency, with harmonics within the range of interest. However, at atmospheric pressure, the air flow necessary to produce such a high input velocity would surpass 80 m/s, an input velocity well above our highest design velocity. Given that bat

activity is significantly reduced at wind speeds above 6 m/s, and that tip-speed ratios on wind turbines average 7 to 8, we propose to design our prototype for maximum blade speeds of 42-48 m/s.

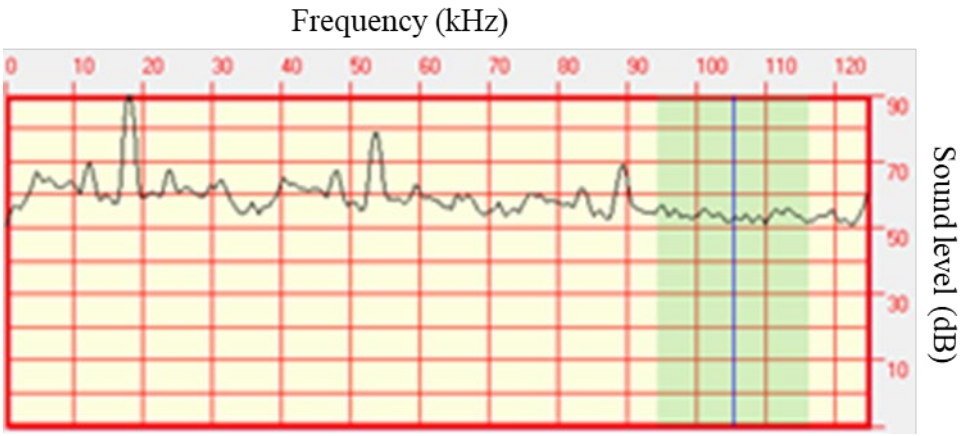

Fig. 6. Spectrogram of the tested dog whistle using pressurized air at 18 psi.

To test the dog whistle at lower flow velocities, a second series of tests was conducted in the UMass wind tunnel. The wind tunnel has a cross sectional area of 1 m × 1 m, is capable of producing air speeds of 2-22 m/s, and has a turbulence intensity of less than 1.0%. The turbulence intensity was calculated as the ratio of the root mean square of the velocity fluctuations to the mean of the free stream velocity, at several wind speeds and locations in the test section. Figure 7 shows a sample of a flow profile and its corresponding turbulence intensity measured at a wind speed of U = 7.8 m/s. At this wind speed, the flow is suitably consistent so that pilot measurements are reflective of the flow velocity throughout the cross section of the wind tunnel.

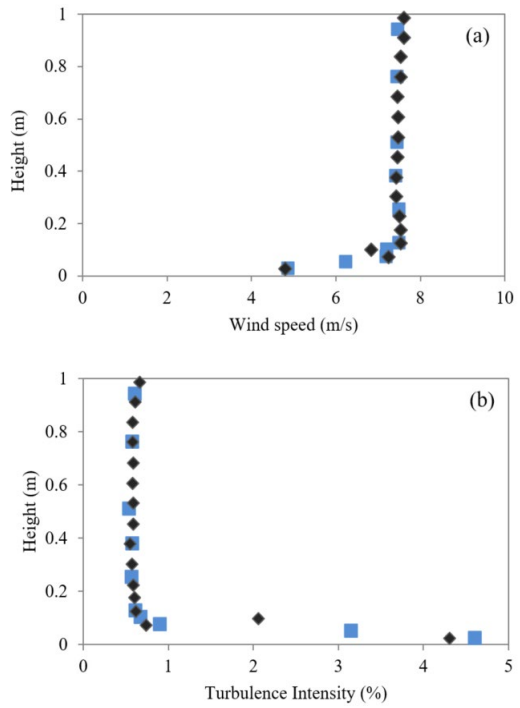

Figure 7. Sample measurements of the (a) flow profile and (b) turbulence intensity at the wind tunnel test section. Symbols represent two series of tests.

The dog whistle was fixed to a plate, positioned perpendicular to the wind flow, and placed in the test-section of the wind tunnel. The sound produced was recorded by the AR125 microphone placed 2 cm downstream of the whistle. Flow velocities tested were in the range of 3-20 m/s, and Figure 8 shows whistle responses for air velocities of 4 m/s and 20 m/s. As shown in these figures, no distinct peak was observed in the frequency range desired (>20 kHz). These results were consistent throughout the 3-20 m/s velocity range. From these results, we conclude that in order to achieve frequencies in the ultrasonic range with a dog whistle, it is necessary to have an input flow rate greater than can be expected on a wind turbine blade.

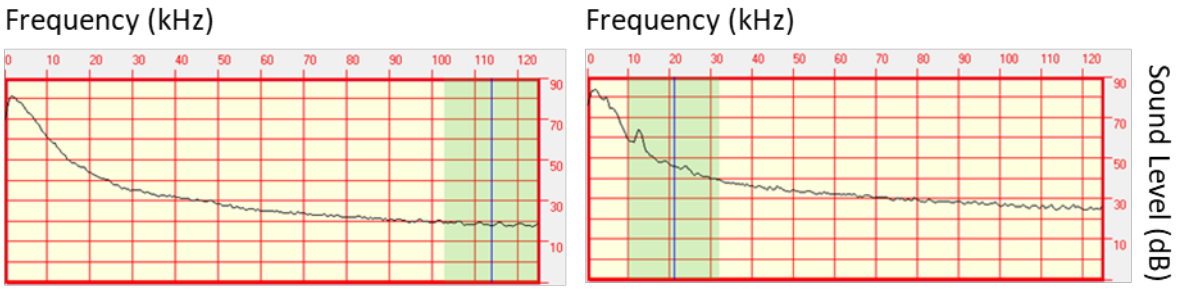

Figure 8. Spectrograms of the tested dog whistle in the wind tunnel at a) 4 m/s and b) 20 m/s flow.

BAT LARYNX MODELING

The larynx of the greater horseshoe bat (*Rhinolophus ferrumequinum*) represents an appropriate initial model for the production of ultrasound. Kobayasi et al. (2012) described the patterns of ultrasound produced by an excised larynx of this bat, but unfortunately did not describe the anatomy of the larynx. We requested this information from the authors, but they were unable to provide us with a 3-dimensional model of the larynx, or details on its dimensions and shape. However, we were able to gain access to specimens of this species, and other bat species that were preserved in ethanol at the UMass Natural History Collections. Initially, we chose to model the internal laryngeal geometry of three species. The Geoffroy's horseshoe bat (*R. clivosus*), which is in the same genus as the greater horseshoe bat, and presumably has similar laryngeal anatomy, and two Vespertilionid species, the eastern red bat (*Lasiurus borealis*) and the pallid bat (*Antrozous pallidus*). Both species produce frequency-modulated calls, with maximum frequencies of >50 kHz, and minimum frequencies of about 40 and 30 kHz respectively. The pallid bat is unique in that it also produces loud social calls which are audible to humans (Arnold and Wilkinson 2011). We felt these species would provide a range of structures used across bat taxa for generating ultrasound.

We conducted micro-CT scans of the three bat specimens using the micro-CT scanning system at the Harvard Center for Nanoscale Systems. Micro-CT is a non-destructive X-ray imaging technique capable of generating 3-dimensional, cross-sectional and internal structure images. This technique uses micro-focused X-rays to create a shadow image of an object based on X-ray absorption by the material. Computer software then processes images and reconstructs the 3-dimensional structure of the object from the intensity values in the projected shadow images, with micrometer resolution.

This system is typically used for visualizing dense substances, such as bone or cartilage. However, we were able to use the system to generate a 3-dimensional model of the empty air space within a specimen's lungs, trachea, larynx, and pharynx. The initial model was quite rough, and required significant editing to create a "water-tight" model in which all surfaces were continuous, and the air space was contained rather than connected with the outside air space surrounding the specimen. Using Imagine software, a reconstruction program tailored for manipulating these models, we were able to reduce the model to solely negative air space and interpolate a 3-dimensional stereolithographic (STL) body for the *R. clivosus* specimen. The other two specimens appeared to have less well-preserved larynxes, so they may not provide an accurate reproduction of the laryngeal anatomy. We have not edited and evaluated the models from these two specimens, but they may not be usable for our purposes.

For the *R. clivosus* specimen, we filtered the 3-dimensional STL body to reduce superficial variance inherited from the digitization process. Figure 9 shows a 3-dimensional model of the negative air space within the bat's airway in light blue, with the soft tissue of the bat's head visible in the background. We were able to print the final product at several scales (larger than actual size) in acrylonitrile butadiene styrene (ABS), using our in-house 3-dimensional printers. We found the print resolution was adequate for printing in detail sufficient to readily distinguish the trachea, air sacs, and pharynx. Because it models the negative airspace outlined by laryngeal tissue, rather than the tissue itself, it is impossible to know from this technique the proper thickness of the laryngeal tissue. In addition, the slight variations that arose in the STL interpolation process (Fig. 10) resulted in a resolution that was too coarse for computational fluid

dynamics (CFD) modeling. While the 3D printer created a smoothing effect due to a higher dimensional tolerance, the numerical mesh is too sharp compared to the natural larynx, particularly in the region where the ligaments would be located. However the other surfaces are well defined and a good starting point for the meshing procedure necessary for CFD. Noting that the STL body is in fact a negative volume, simply cutting it from an arbitrarily larger solid is an easy solution that would allow us to use the CT imagery in conjunction with higher resolution alternative sources, not produced from negative air space. Thus it may be possible to overlay this geometry with a higher resolution ligament model, from a mechanically similar larynx, to give us a complete vocal track to model.

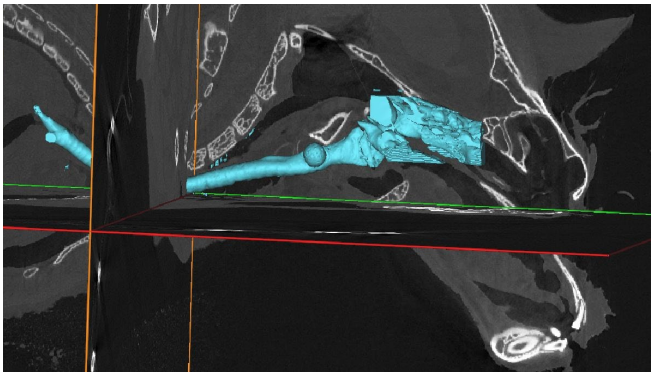

Fig. 9. Three-dimensional model of a bat airway overlaid on parent CT scan section of the bat head. Negative air space is visible in blue, bone and cartilage in white, and soft tissue in gray. The airway model shows, from left to right, the branching of the trachea to enter each lung, the trachea, round air sacs, larynx, and pharynx. The ear of the bat is visible in the upper right, and eye socket and muzzle, mid and lower right.

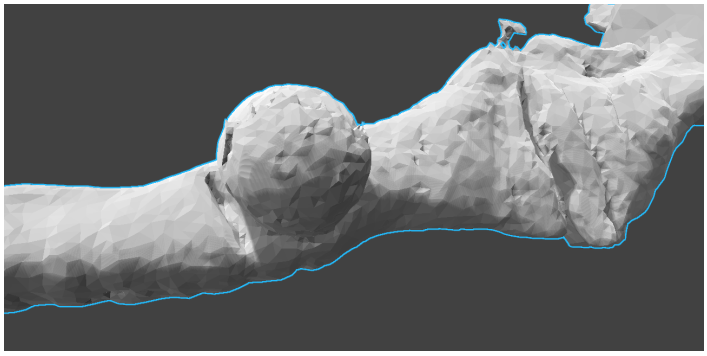

Fig. 10. Detail of surface tessellation on 3-dimensional larynx model after filtering high frequencies. The interpolation errors are still too great for CFD.

FROG LARYNX MODELING

Obtaining a Model

The concave-eared torrent frog is the only frog species known to produce ultrasound and provides an alternative to the bat larynx model (Suthers et al. 2006). Suthers et al. (2006) provide cross-sections of the male torrent frog larynx through the mid-portion and dorsal third of the vocal cords. The mid-portion is described as characteristic of the vocal cords along much of their

length. As a preliminary simplification, we took the mid-portion section and digitized the outline of the vocal cord with a calibrated data extraction suite for Matlab (Fig. 11). Revolving the digitized mid-section allowed us to design our first larynx prototype (Fig. 12). Because the actual larynx was only a few micrometers in length, we used a scaling factor to enlarge the prototype to a size appropriate for experimental analysis. The larger prototype also allows for greater air flow, and thus makes it easier to attain ultrasonic frequencies.

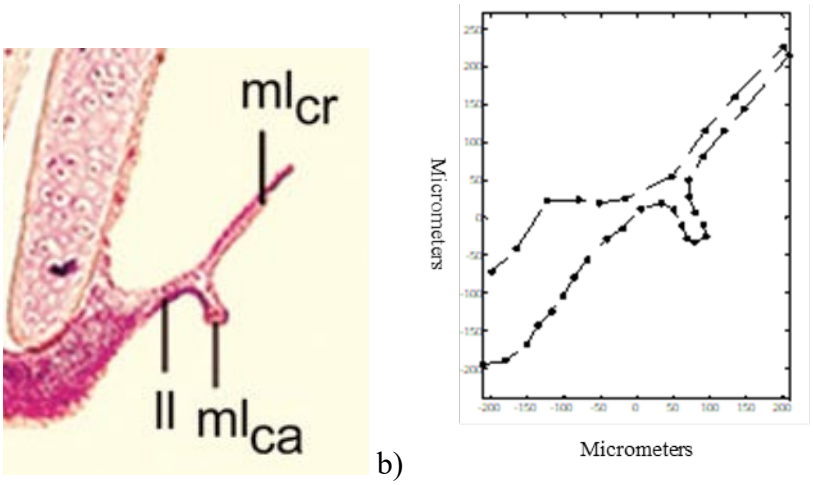

Fig. 11. Midportion cross-sections of torrent frog vocal cord from a) Suthers et al. (2006), and b) digitized by our team. In 7b, units are in micrometers.

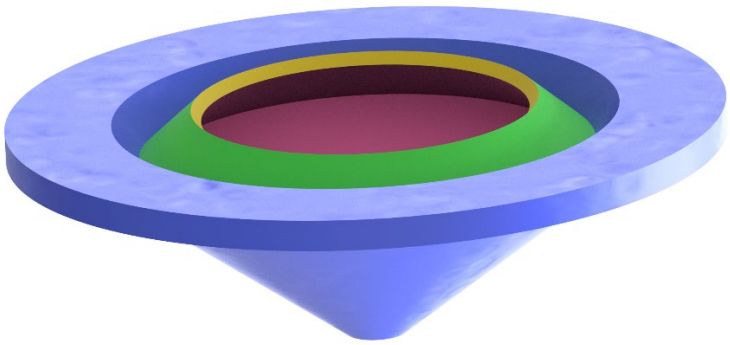

Fig. 12. Rendering of the simplified frog larynx prototype, based on a revolved midportion cross-section.

We designed an axially asymmetric larynx model that more closely resembles the actual larynx geometry. This model will incorporate changes in the vocal fold shape as we move from the mid-portion to dorsal-third sections (Fig. 13). Interpolation between the mid-portion and dorsal-third sections will be done by linear lofting between fixed sections, followed by smoothing of unnaturally sharp edges of the resulting facets. After the dorsal third section, both sides will converge until the section is closed.

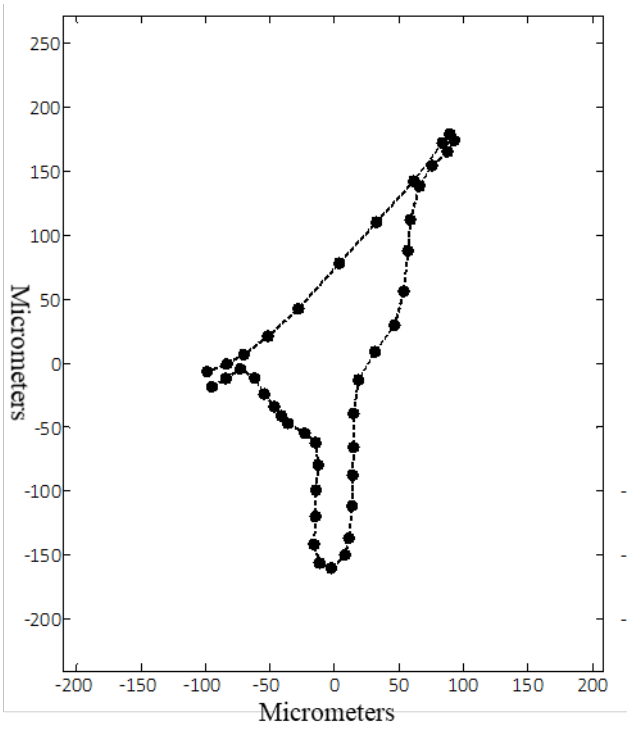

Fig. 13. Dorsal third cross-section of torrent frog vocal cord from as digitized by our team. Units are in micrometers.

Flexible Casting

To develop a physical larynx model, our next step was to identify a flexible material that could give us control over the geometry of the structure produced, have appropriate structural flexibility and damping, and could be easily manufactured. Existing technologies that allow for the production of flexible structures with variable geometry include UV-cured Inkjet 3D printers. The Objet/Stratasys and the 3D Systems 5500X printers both print a variety of flexible materials, but these materials are viscoelastic, and have high structural damping. We tested samples of these materials and found that their high damping qualities prevented production of ultrasound. As a result, we began casting models of flexible material in 3-dimensional printed molds of the desired geometry. We used an in-house printer for printing molds, the Stratasys Eden260, with a 255 x 252 x 200 mm bay and 20 micron accuracy, and used silicone manufactured by Smooth-On, Inc. (Easton, PA) for our flexible material. In order to find the elasticity modulus of the structure, we first cast a circular cylinder out of silicone material. Following the method described by Paidoussis (2014), the elasticity modulus was experimentally measured as E = 20 kPa. This value falls within the range of structural flexibility for the animals of interest, E~20-40 kPa.

We first tested the flow-induced oscillation of the silicone using a thin membrane with a uniform thickness of 3 mm. The membrane was stretched over the circular inlet of a cylindrical tube, and slit in half to mimic experiments using a synthetic human vocal fold model. The ultrasonic microphone was placed downstream of the flexible membrane to record the sound emitted by flow-induced vibration of the flexible membrane. Figure 14 shows a sample frequency response

for the sound measured downstream of the flexible membrane, using an input pressure of 18 PSI. As shown in the plot, the frequency measured from the flow-induced oscillation of the membrane shows a broadband frequency response in the range of 5-35 kHz, with the maximum amplitude of 70 dB at 5 kHz. Our observation of a high frequency response from the flow-induced vibration of the silicone membrane is encouraging and demonstrates that our manufacturing technique is effective. The silicone model will require further modification since the high frequency response was only observed under a high flow velocity that does not exist on a wind turbine blade.

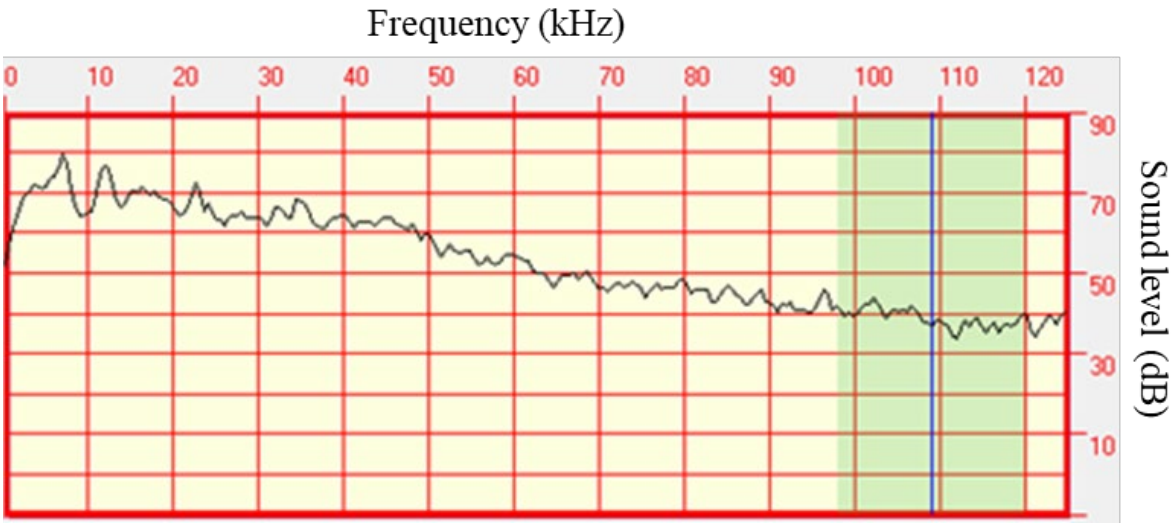

Figure 14. Spectrogram of the tested flexible membrane using pressurized air at 18 psi.

We used the CAD model as a negative volume and were able to design a series of casting molds that could be used to produce future larynx models (Fig. 15). With the Stratasys Eden260 3D printer, we can produce a mold with excellent surface tolerance, and with a very quick turnaround from schematic to physical model. Traditional casting methods, however, did not anticipate the porosity of the printed ABS material. Normally, a thin film of de-molding oil assures clean separation of the work piece from the mold. In our case, however, the ABS entrains the oil before the silicone solidifies, allowing the silicone to infiltrate the mold, and damaging the final surface. Through iterative testing, we determined that saturating the mold first in water and then with layers of de-mold grease for 24 hours before casting alleviates this issue. Thus we finalized an approach to cast larynx geometries of variable size and shape. We used our finalized approach to print two larynx prototypes, with one at 1/27th the solid volume of the other (diameters approximately 1 cm and 3 cm respectively) (Fig. 16). These prototypes represented the simplified geometry described previously – that is, the midportion section of the torrent frog larynx was digitized and revolved to produce an axially symmetric larynx. Our next step will be to use our established molding techniques to produce the axially asymmetric larynx model, which is a more accurate characterization of the torrent frog larynx. While the multi-faceted body is much more complex than the simplified revolved mid-portion larynx, on-going work to design the appropriate mold has been successful (Fig. 17).

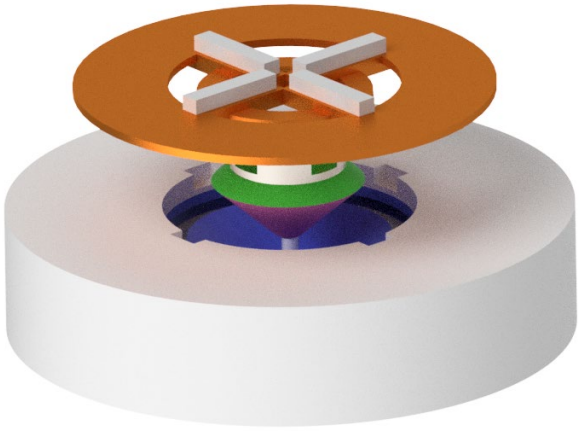

Fig. 15. Mold assembly for the simplified prototype larynx in false color.

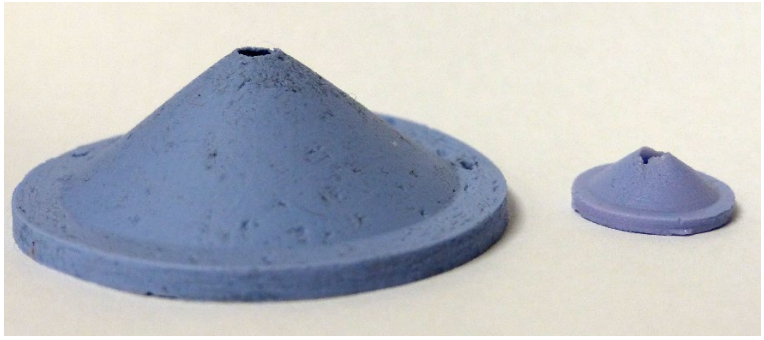

Figure 16. Cast prototypes at two spatial scales.

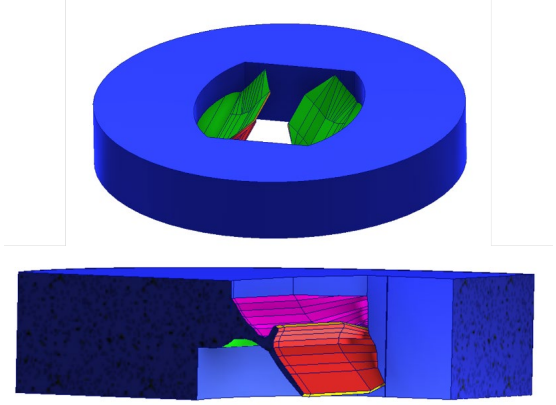

Figure 17. Proposed model of axially asymmetric larynx, which better represents torrent frog vocal cords.

Simplified Larynx Response to Wind Tunnel Flow

Peak air flow rates produced by pressurized air lines can be significantly higher than those measured on wind turbine blades, thus we decided to test our larynx models under more realistic

conditions in a wind tunnel. Initially, we used a wind speed of ~20 m/s, which is near the upper range of our design wind speeds. The larynx model was affixed to a rig setup (Fig. 18) to reduce structural excitation, with the AR1225 ultrasonic microphone placed 2 cm downstream of the larynx outlet. Pitot measurements were taken 10 cm above the setup to establish the flow velocity for each case, well out of the boundary layer of the wind tunnel. In initial tests, we observed ultrasonic peaks in the resulting spectrograms, however, in a follow-up setup with the larynx inlet blocked, we observed similar peaks, suggesting that the ultrasound resulted from vortice shedding around the fixing plate on the rig setup (Fig. 19). We believe these vibrations resulted in harmonics throughout the ultrasonic range.

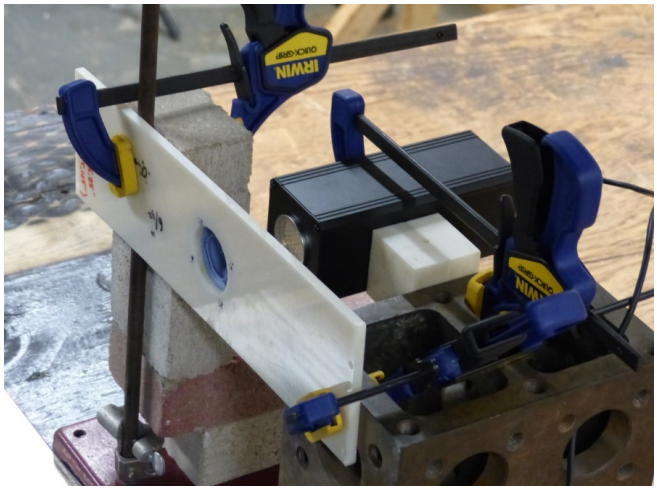

Fig. 18. Experimental setup for wind tunnel testing, with larynx (light blue) attached to white plate, upstream of the microphone.

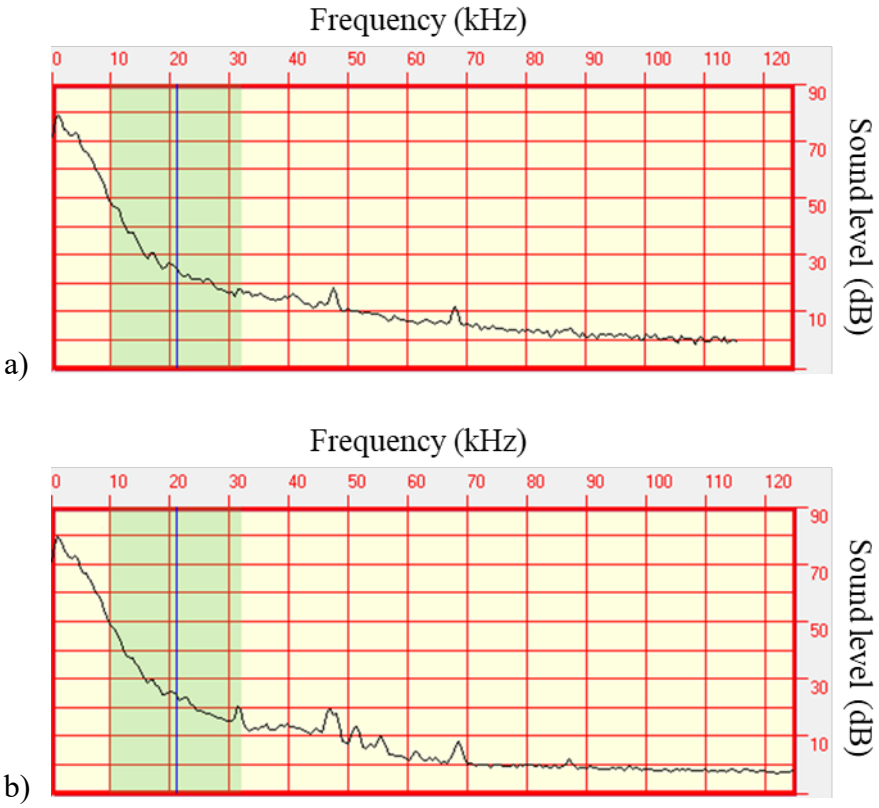

Figure 19. Spectrograms of prototype larynx in 16 m/s flow in wind tunnel with a) larynx open, and b) larynx blocked. Ultrasonic peaks are due to vortex shedding around rig, and not due to oscillations of the prototype device.

OTHER VELOCITIES

We designed a simple flow concentrator to increase air flow to the larynx device. The concentrator had an aspect ratio of 1 inlet diameter, with a circular inlet of radius 23 cm and outlet radius of 4.5 cm. Free stream tests returned an average flow rate increase of approximately 15%. We conducted the same test as described above, but with the flow concentrator in place immediately upstream of the larynx model. This test yielded a jet flow which did actuate the larynx and induce vibration, observable with a high-speed camera separate from the flow and focused on the upstream ligament. However, vibrations were not discernable at a frequency within the ultrasonic range. The concentrator design increased the flow rate by approximately 15% for this flow range (~20 m/s), but the change in larynx response was much greater than from previous similar velocity increments. This is likely due to the concentrator decreasing the standoff distance between the larynx and the stagnation point, letting the jet impact the larynx in a way the normal flow would not.

Flow Stagnation Visualization via Water Tunnel

We theorized that one reason the larynx was not being actuated was that the flow was stagnating before encountering the larynx structure. To test this idea, we conducted flow visualization in water at a lower Reynolds number. This approach is reasonable even though water is

incompressible, because the air flow of interest is far lower than the near supersonic speeds at which compression effects dominate. Even at a lower Reynolds number we observed full stagnation approximately 0.5 larynx diameters upstream of the larynx structure, as indicated by ink streamlines not passing through the interior channel of our prototype. This finding, along with the shedding frequency analysis conducted earlier, point to the need for additional controls on the flow in order to direct flow through the larynx structure. Future tests to fine-tune the larynx placements will be conducted in a custom built flow concentrator where we have better control over the pressure gradient across the larynx section.

Computational Fluid Dynamics Analysis

In the experimental environment, recording the physical response of the larynx can be limited by instrumentation, but not computationally. In the initial portion of our study, we modeled a simplified axially symmetric larynx, which was then used throughout the experimental phase. This structure was tested in various computational fluid dynamics (CFD) suites and solvers, including the laminar and turbulent approximations for both ANSYS Fluent (Fig. 20) and OpenFOAM (Fig. 17). Here we developed several solutions which matched the expected Reynolds number for the device placement on a wind turbine blade. The asymmetric jet (Fig. 20) agrees with experimental flow visualization conducted by Sidlof et al. (2011) and for a transient solution of higher Reynolds flow the jet tended to oscillate across the downstream section. Of particular interest is the entrainment of the boundary layer flow to the central section vortex (Fig. 21). In the axially asymmetric model, we anticipate that the shorter aspect ratio ligaments of the 1/3rd section would intercept this entrained flow, possibly allowing for greater control throughout the larynx without the need for tensioning the entire length.

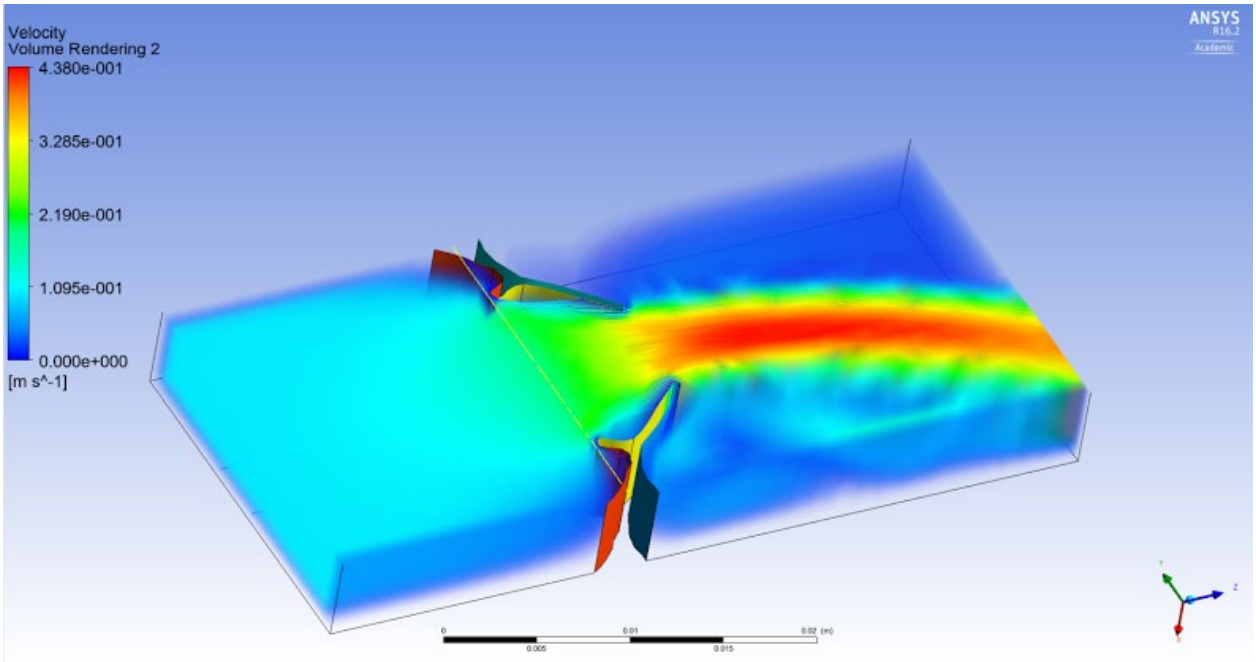

Fig. 20. ANSYS Fluent simulation at Reynolds number 2400.

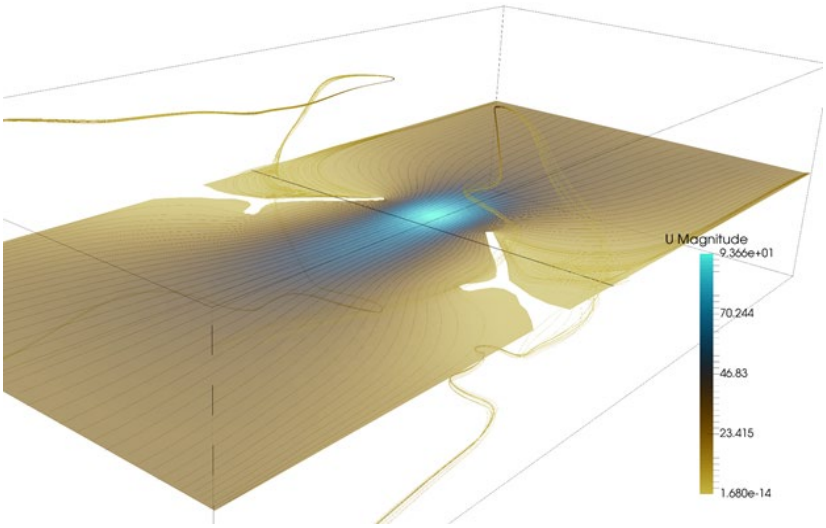

Fig. 21. OpenFOAM simulation at Reynolds number 3000.

Figure 22 shows the numerical mesh used in the OpenFOAM simulations and the pressure contours seen at the trailing tip during flow initialization of the same case from Figure 20. This movement of the separation point upstream is in agreement with established Particle Image Velocimetry (PIV) measurements by Sidlof et al. (2011) who observed a flow separation further downstream immediately before and after glottal action for a Reynolds number of similar magnitude (5,400).

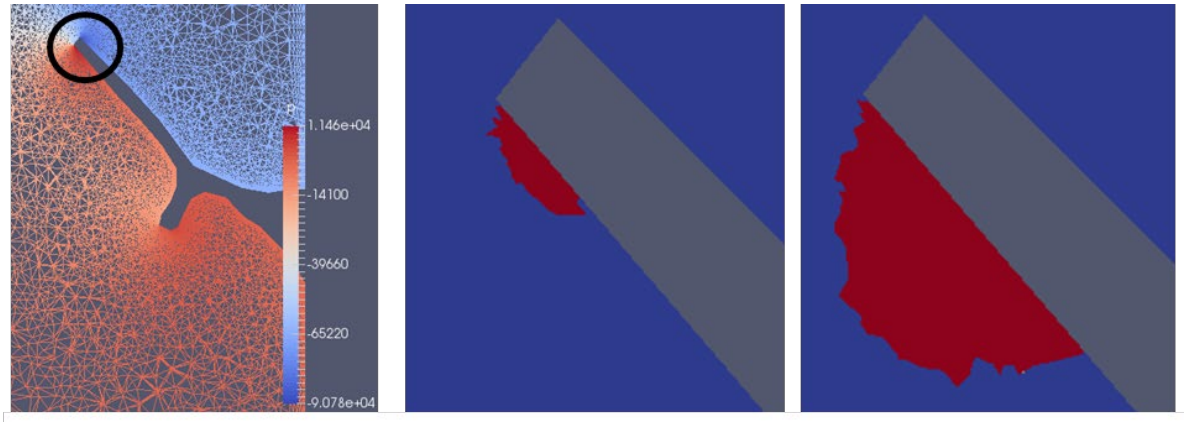

Fig. 22. Mesh refinement (a), and pressure contours (b and c) along trailing tip during flow initialization.

FUTURE WORK

We have designed and cast an axially-asymmetric version of the torrent frog vocal cords. The lack of revolved features in this design means that hundreds of STL faces must be manipulated by hand to attain a working mold model, as opposed to the initial prototype in which we used a

simplified revolved design. Future prototypes will also require structures which may be composed of multiple materials, allowing us to apply tension to increase the frequencies produced by these flexible structures. In nature these larynx mechanisms are not actuated by muscles, but rather tension is applied to local regions of the ligaments, and non-homogenous materials will allow us to achieve this.

We have also designed a new concentrator that will allow implementation of varying aspect ratios at the inlet of the larynx model. This allows use of a wider range of input flow velocities with the device. In addition, the use of a concentrator insures that the flow stream is directed through the device, rather than being directed around the device, or stagnating in front of it.

We have developed a small-scale wind tunnel set-up (see Sidlof et al. 2011), which allows us to better control and measure input and output parameters. In addition to using this set-up to test a variety of flexible larynx designs, this system can be used to test existing rigid deer and dog whistles, to determine whether these systems should be pursued further. We found that the pressurized air-line in the laboratory could not provide the fine-scale adjustments in pressure inputs necessary for carrying out experiments relevant to the design air pressures and air flows of interest. In addition, the UMass wind tunnel was not ideal for testing due to restrictions on scheduling use, and the amount of effort needed for sufficiently rigid setups.

In summary, our initial work has focused on an experimental approach rather than full development of multiple digital models. Our literature review suggested that a variety of thin, flexible, asymmetric structures are capable of generating nonlinear ultrasound.

Task 3: Develop series of prototype whistles operating over a range of frequencies: 25-35 kHz, 35-45 kHz, and 45-55 kHz range.

TASK SUMMARY

Initial deterrent prototypes were tested for transient flow conditions (Fig. 23). It was observed that acoustic higher harmonics are generally observed for most larynx geometries, far surpassing the acoustic emission range we initially hoped for. Task 3 milestones deal with designing different deterrent prototypes encompassing frequency-modulated ranges of 25-35 kHz, 35-45 kHz, and 45-55 kHz. Ongoing testing regarding axial tension has been successful in widening the acoustic spectrum, with higher tensions making the response more broad-banded. Note in the threshold plot (Fig. 24) that by controlling the tension, we can control the higher harmonic emissions such that the low-frequency range is dominant (i.e. cases below ~0.3 Newton, or N, tension), evenly distributed (0.75 N – 1.5 N), or merged into a full spectrum response (>1.75 N). This tension continuum, while not the three distinct prototypes as envisioned in the original SOPO, accomplishes the same goal insofar as we can designate different pre-tensions (a constant value, thereby a separate device prototype) to make the whistle more effective for the lower flow velocities encountered closer to the root of the turbine blade. Separate from widening the frequency range, we have also studied the temporal frequency-modulation within the signal. First

seen in Budget Period 1 (Fig. 25), and expanded our research to alternate geometries and materials to determine what system parameters this phenomenon is dependent on. For a low density polyethelene (LDPE) "flag" in flow, it was observed that the periodicity of frequency modulation directly corresponds to the fundamental flag flapping frequency, and that the same frequency can be seen in the acoustic higher harmonics. We refined a tension rig: for the linear larynx model we previously observed a reduction in the flow velocity required for the onset of oscillation at one particular tension but were unable to replicate this result. Interestingly, early reports indicate that the pre-tension is an effective way of limiting the *maximum* operating velocity of the deterrent, as oscillations cease when the film buckles. See the midpoint of the spectrogram in Fig. 26, which corresponds to approximately 30 m/s (the velocity is ramped from 0-30 m/s and reversed). Distinct harmonics are suppressed within the 7-9 second window. The buckling velocity has thus far shown to be highly dependent on the axial tension and does not appear for cases below 10% strain. If the proper conditions are replicated for the deterrent prototype, we may be able to add this as an additional deterrent functionality preventing the whistle from operating during high-wind scenarios. Bat flight is reduced in winds higher than approximately 6 m/s, thus preventing the whistle from oscillating in these higher winds is beneficial both to the fatigue life of the larynx geometry, and to preventing potentially unforeseen acoustic emissions at very high flow velocities.

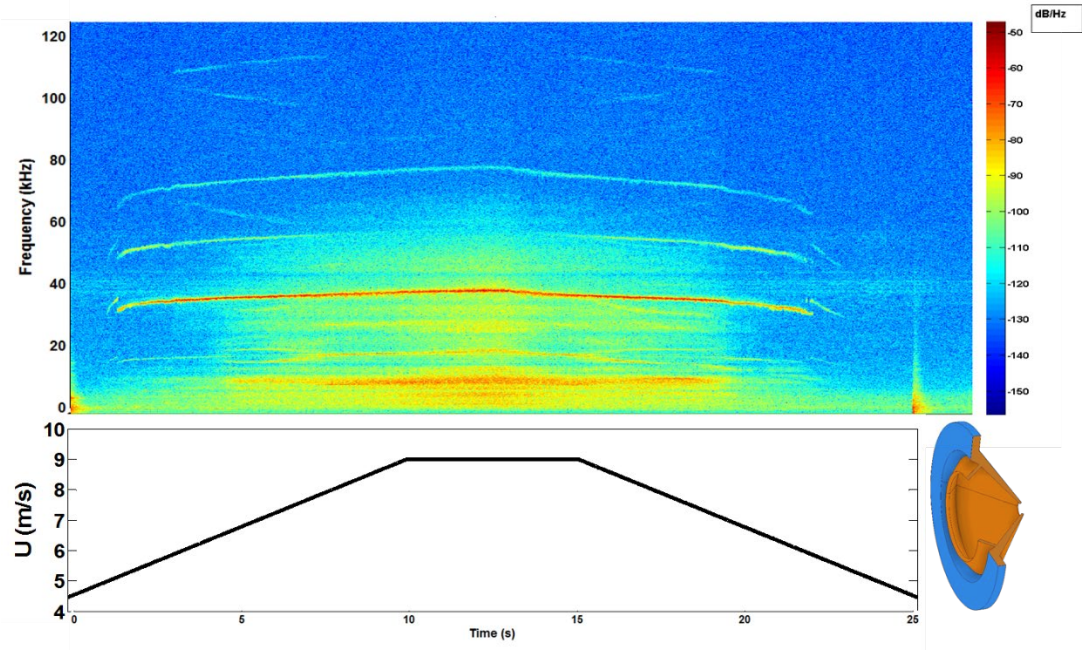

Fig. 23. Response of a revolved larynx to transient flow velocity.

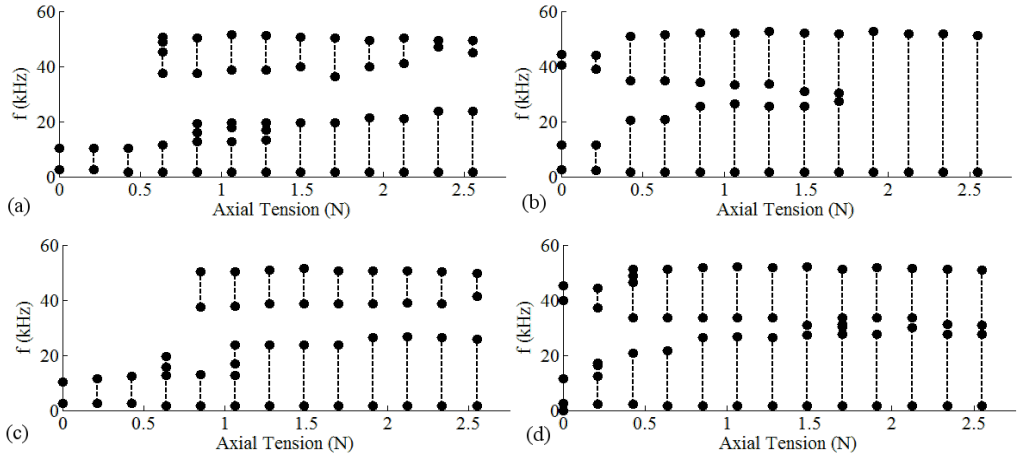

Fig. 24. Acoustic spectra contours with a 50 dB cutoff, for a linear larynx under varying tensions and velocities. (a) 9.6 m/s, (b) 12.3 m/s, (c) 14.9 m/s, (d) 17.5 m/s.

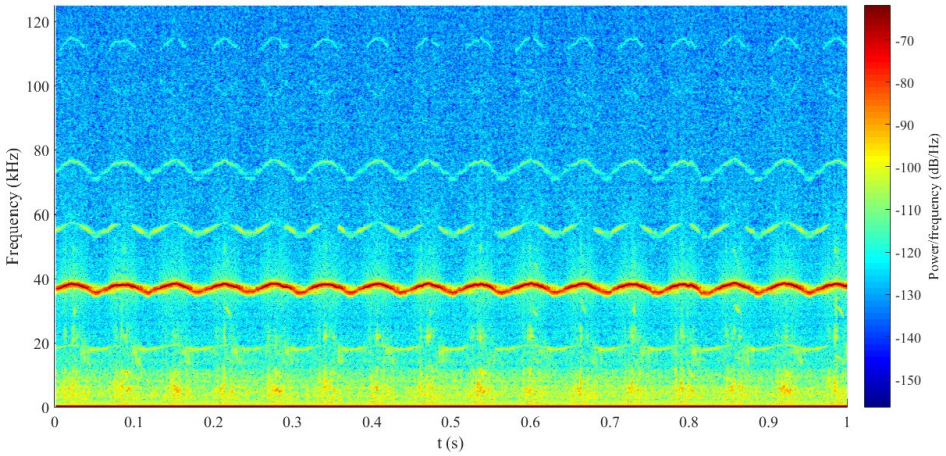

Fig. 25. Budget Period 1 results for frequency-modulation.

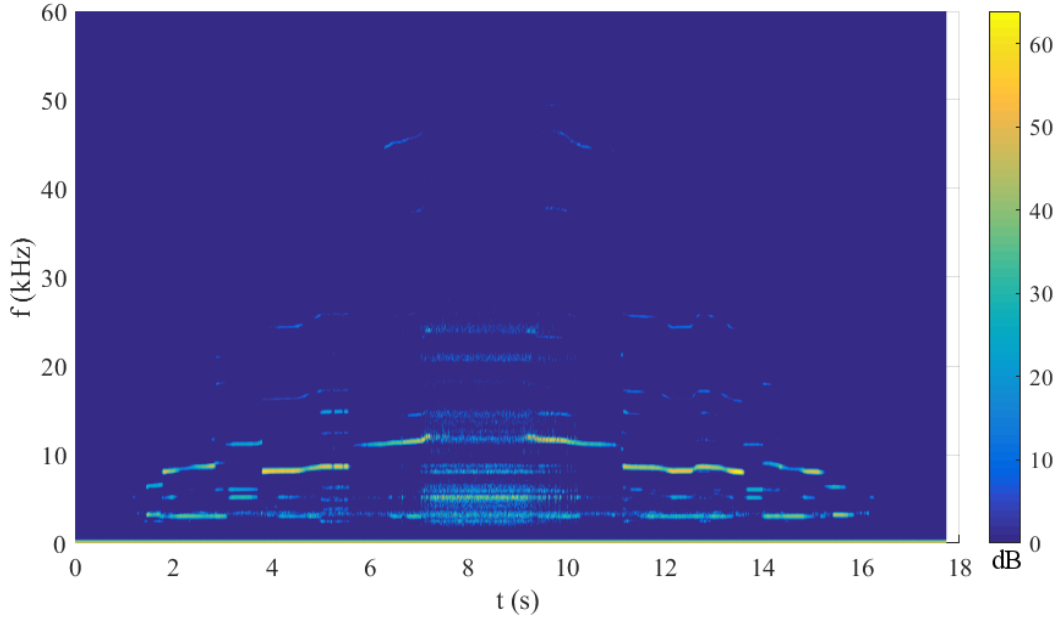

Fig. 26. LDPE flag in ramped flow with 30% strain.

We expanded our research to alternate geometries and materials to determine what system parameters this phenomenon is dependent on. For a low density polyethelene (LDPE) "flag" in flow, it was observed that the periodicity of frequency modulation directly corresponds to the fundamental flag flapping frequency, and that the same frequency can be seen in the acoustic higher harmonics. Our refined tension rig is shown below (Fig. 27):

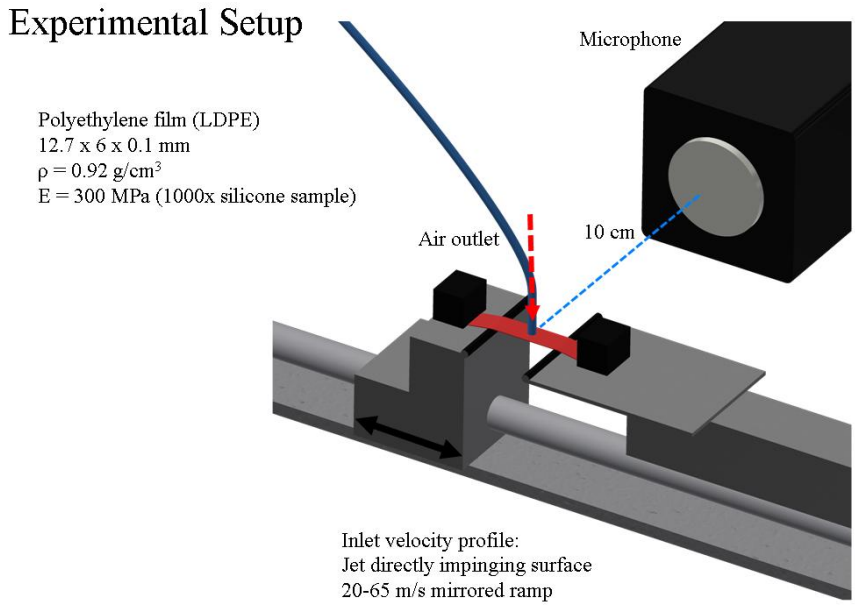

Fig. 27. Experimental setup for testing ultrasound production.

• At low strain, frequency jumps are possible for lower velocities and constant tone at higher velocities 0% strain LDPE, transient flow (Fig. 28).

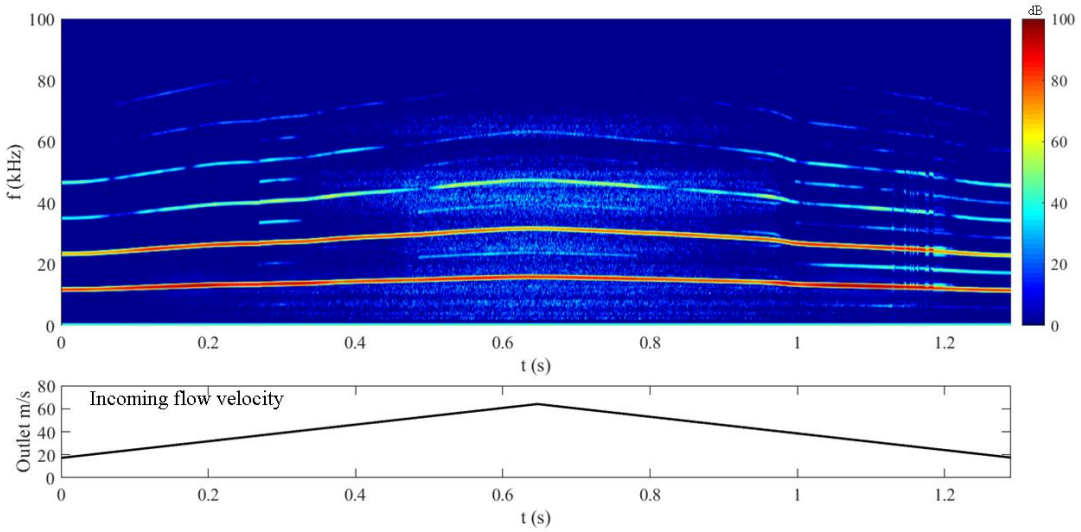

Fig. 28. Results from a low strain test showing that frequency jumps are possible at lower velocities and constant tone.

• Higher tension shifts the dominant harmonic to ultrasonic with a 15% tension increase of the LDPE in transient flow (Fig. 29).

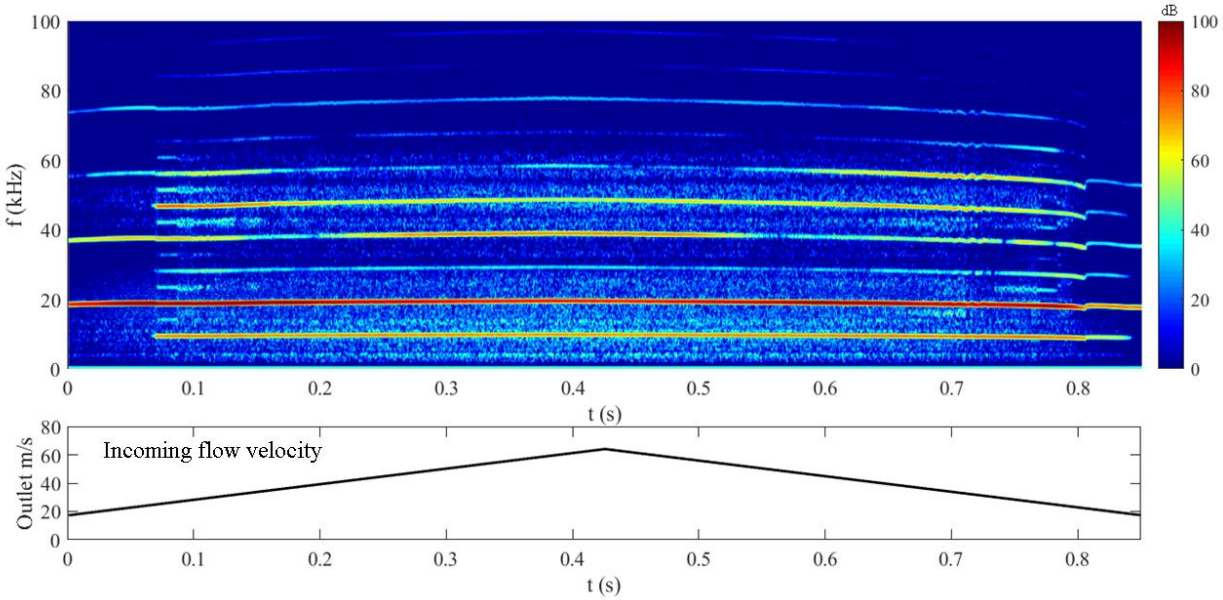

Fig. 29. Results showing at higher tension, there is a shift of the dominant harmonic to ultrasonic.

• On a longer timescale, frequency jumping occurs within the harmonics, to hysteretic subcritical band (dashed) with a 15% tension increase in the LDPE and a transient flow at 16x (Fig. 30).

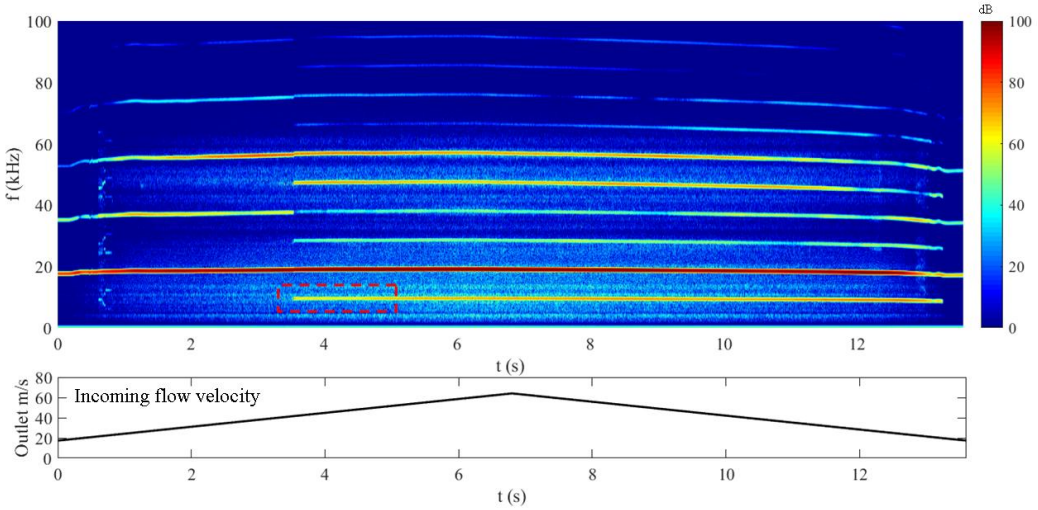

Fig. 30. Results showing that on a longer time scale, frequency jumping occurs within the harmonics.

• At 60% tension, there is a constant tone regardless of flow.

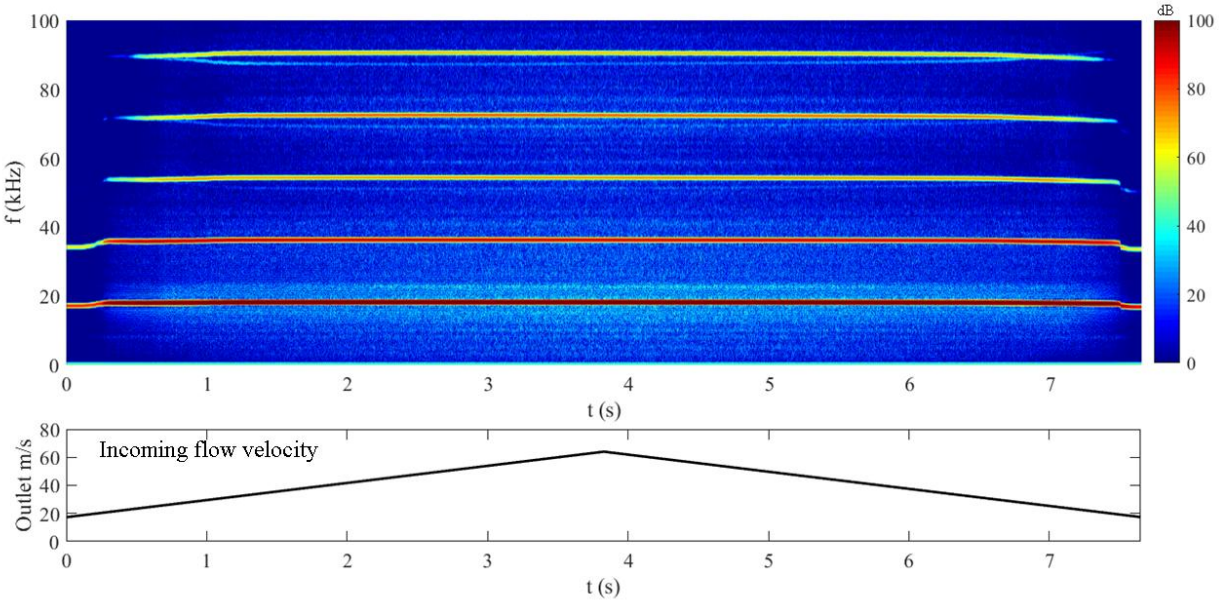

Fig. 31. Experimental results showing that at 60% tension, there is a constant tone regardless of flow.

Whistle Design Conclusions:

• Complexity of larynx geometry can be reduced to a tensioned film in flow.
• Our device produced ultrasound using flow-induced oscillations, in the desired frequency and power range.
• Tension effectively controls harmonic frequency and hysteretic characteristics.
• There is a 95 dB peak at 10 cm that corresponds to a 61 dB peak at 5 m from the whistle.

Task 4: Complete research to develop the frequency, intensity, and pattern specifications that leads to deterrence of free-flying bats.

TASK SUMMARY

During April through June 2019, we tested the effect of our ultrasound recordings on bat behavior, using thermal imaging videography, as described in our Updated Biological Study Design (see Task 7, Deliverable 6, below). Recordings were made on rainless nights from 9 PM to 2 AM, though most bat activity occurred prior to midnight. We analyzed 100 hours of video collected from the rooftop experimental arrays and found that, even though our microphones picked up calling bats, the cameras showed that all bats were at least 100 meters overhead. This height was beyond the range of our broadcasting speakers, and thus we were unable to evaluate the effectiveness of the ultrasounds on their behavior. In our preliminary work we had assumed that bats were flying within range of our speakers because we frequently recorded their calls on our microphones, but apparently they were calling quite loud, while remaining over 100 m from our experimental setup. We were also surprised that none of the bats flew within range, even by chance. We could not point the cameras straight up because their auto-calibrate function does not work with only sky as the background. In addition, our speakers could not project effectively straight up to the height of the bats. As noted before, we observed many instances of bats climbing up very high and then diving down at high speeds, apparently as a means of hunting insects. Because it was unpredictable where this form of hunting behavior would be used, we were unable to capture it in our stimulus sound field.

Due to the high flight altitude of the bats at our rooftop experimental site, we also collected data at an alternate site where bats came and went through a window in an abandoned building, but no strong effects have been detected at this point.

Task 5: Test prototype whistles on wind turbine: We tested our whistle on a small-scale operating turbine blade for up to one week. We compared results obtained from ultrasonic recording in the field with those expected from laboratory testing in the wind tunnel.

TASK SUMMARY

We originally planned to test our whistles on a small wind turbine on the campus of Amherst College, but it became apparent that the size of our whistles relative to the small blades of the turbine could lead to imbalance and a high human health risk if the blades detached. We therefore began testing the whistles on a small turbine in a wind tunnel at UMass that provided a safety net in the event of blade imbalance. The work in the wind tunnel was completed and we then reran our experiments with the deterrent mounted on a rotating turbine case (forced rotation

turbine). This turbine is of similar size to the turbine at Amherst College. Tests were conducted outdoors in order to record relevant background noise. This turbine was safer than the Amherst College turbine because we had full control of the rpms (no free spinning) and the blades were stronger (steel vs. carbon).

Deterrent Performance on a Rotating Scaled Wind Turbine Blade

Introduction

Experiments were conducted to investigate the performance of a bat deterrent in flow similar to that encountered by a full-scale wind turbine blade. A controlled turbine was built to test our deterrents on, which uses a belt drive to force the rotor to spin at known velocities and can use stiffer blades which are less susceptible to mass imbalance. Below we outline the operating parameters of this experimental turbine, the methodology applied, and a performance summary of an air-driven bat deterrent mounted on the tip of a rotating blade.

Forced-rotation turbine

The turbine apparatus we constructed consisted of an electric motor at the base of a small-scale turbine (43 cm hub height) which drives a belt to turn the rotor of the turbine (Fig. 32). The turbine has interchangeable blades, and uses 30 cm circular blades made of steel for maximum stiffness against any load imbalance. The entire system has been designed to safely operate at up to 1000 RPM for a variety of blade masses. While the blades are slightly shorter than the Air-X turbine (30 cm vs 50 cm), having an induced rotation gives us greater confidence in the actual flow velocity at the deterrent, permitting higher rotational velocities and thus the ability to match the linear tip velocity of much longer blades. Since we were interested solely in the device performance for this proposed methodology, circular blades are used in order to keep the aerodynamic loads balanced. The deterrent was mounted on one of the blades, with the other blades counterbalanced by adding tip masses.

Tests were conducted for the turbine with ambient wind present, but the gusts had minimal influence on the microphone for 20 kHz, and was negligible throughout the ultrasonic range. The first orientation of the microphone was facing the rotor plane, such that the deterrent-laden blade traverses a constant angle relative to the center of the microphone beam. Based on the beamform of an AR-125 ultrasonic microphone, Θ_1 was chosen as a compromise between sensitivity decreasing outside the beam against a basic sound propagation model (inverse square). This point comes to $\Theta_1 = 10$ degrees, and given the rotor diameter results in a microphone offset of 1.7 m from the turbine. A series of tests were conducted for this orientation for varying rotor RPM and deterrent mountings. The second orientation, Θ_2, has a microphone on the same plane as the rotor such that a blade tip passes immediately in front of the microphone. A precession was noted in the rotor at higher RPM, so to protect the microphone from a blade strike we shifted it 6.4 cm from the passing tip.

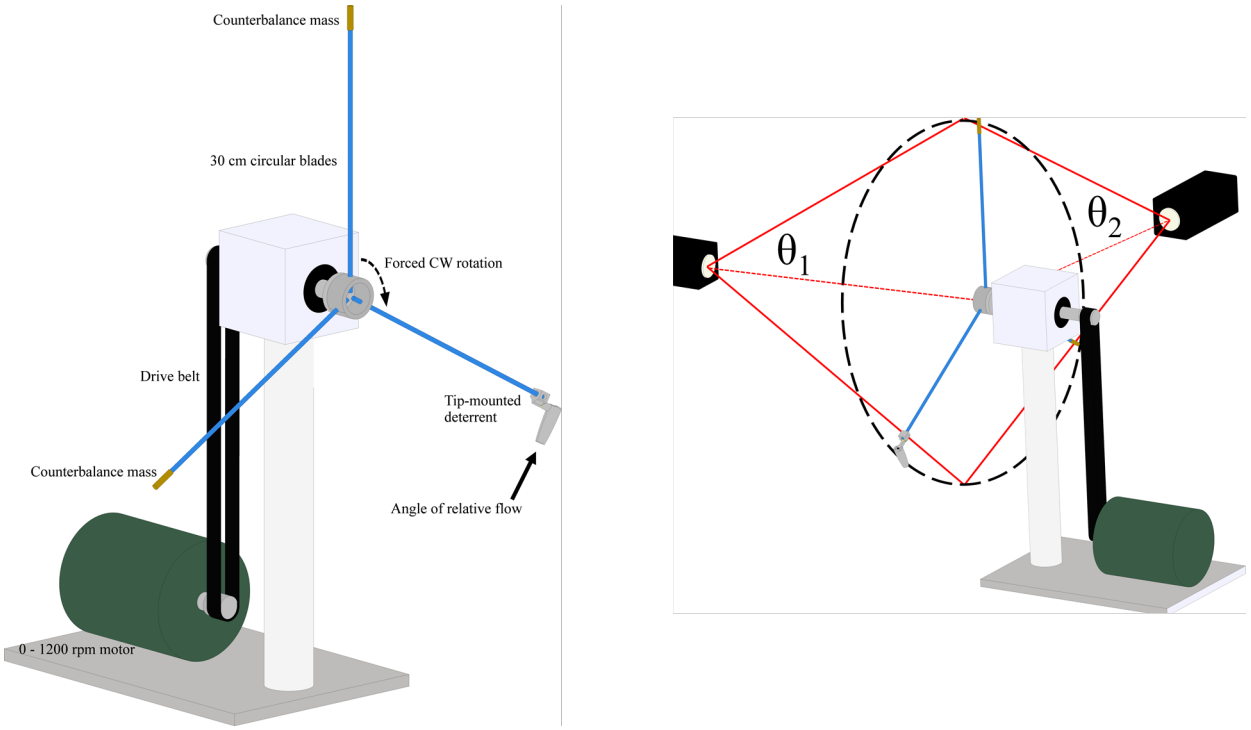

Fig. 32. The belt-driven turbine apparatus. The present work used motor speeds in the 500-700 RPM range, resulting in a tip velocity of 16 – 22 m/s. Θ_1 was 10 degrees, but Θ_2 can reach zero as the deterrent directly passes the microphone, with a maximum value of 45 degrees (with a ~40 dB drop) at the top and bottom of the rotor plane.

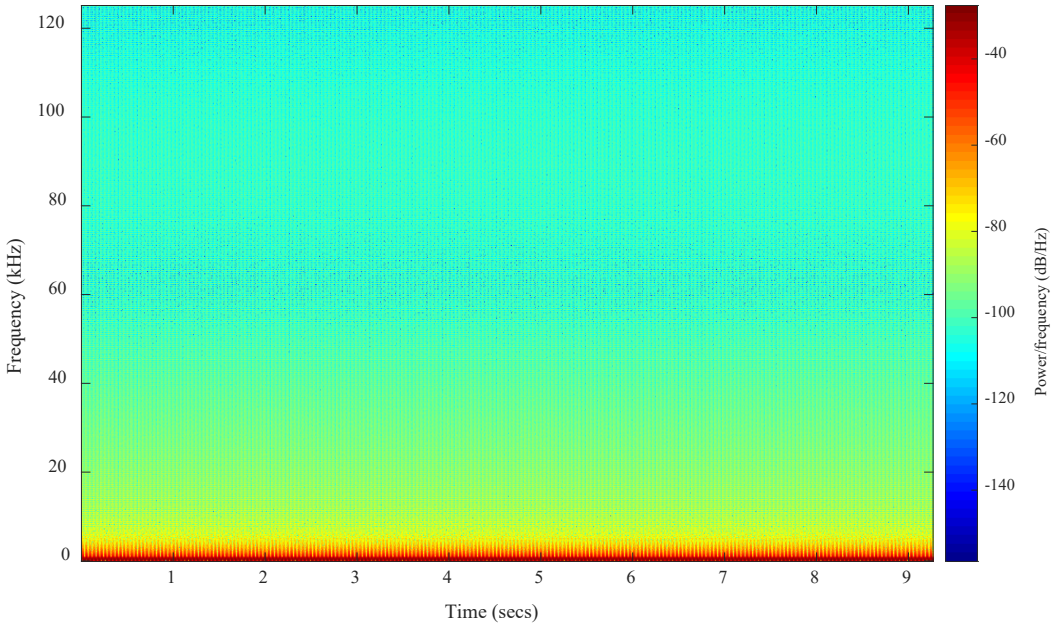

Fig. 33. Background noise. Variations are primarily below 5 kHz, with negligible ultrasonic components.

Θ_2 orientation

Per the methodology previously proposed, the Θ_1 orientation is preferable due to the constant

angle between the rotating deterrent and the microphone beam, but comes with a decrease in sensitivity. Deterrent tests for this case could not isolate an ultrasonic signal which could be attributed to the device, for any rotor speed between 0-700 RPM (22 m/s at the tip), shown in and compared against the baseline noise from ambient wind in Fig. 33. Therefore we prioritized the more sensitive Θ_2 setup (Fig. 34), which gives maximum but time-varying microphone sensitivity. A baseline signal of the turbine operating without a deterrent was recorded (Fig. 35). It was observed that at rotor RPM below the target range, occasional ultrasonic pulses were emitted from the blade with the tip deterrent (Fig. 36), and on a shorter timespan pairs of pulses aligned with the proper blade passing frequency (i.e. two pulses separated by 14 complete revolutions, as seen in Fig. 37). In agreement with the laboratory testing, aligning a film with axial flow results in a response more sensitive to the incoming flow condition, and significantly more ultrasonic pulses were observed when comparing similar timespans. However, this response was also accompanied by a reduction in the acoustic power (Fig. 38).

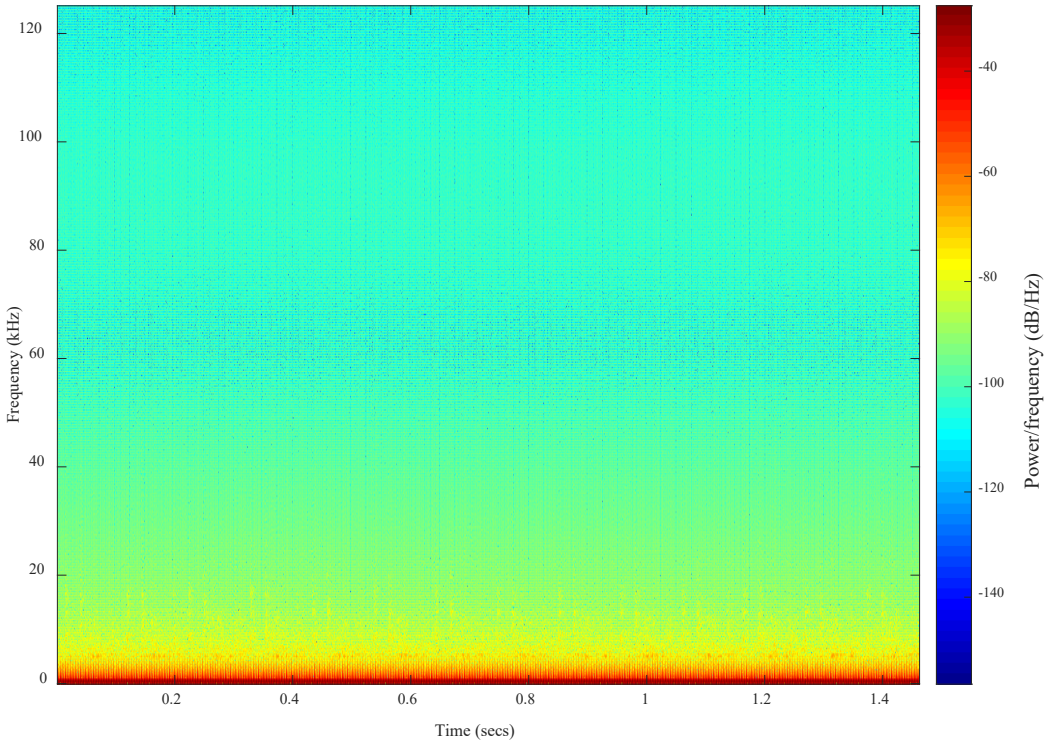

Fig. 14. Θ_1 orientation (1.7 meter offset from rotor plane).

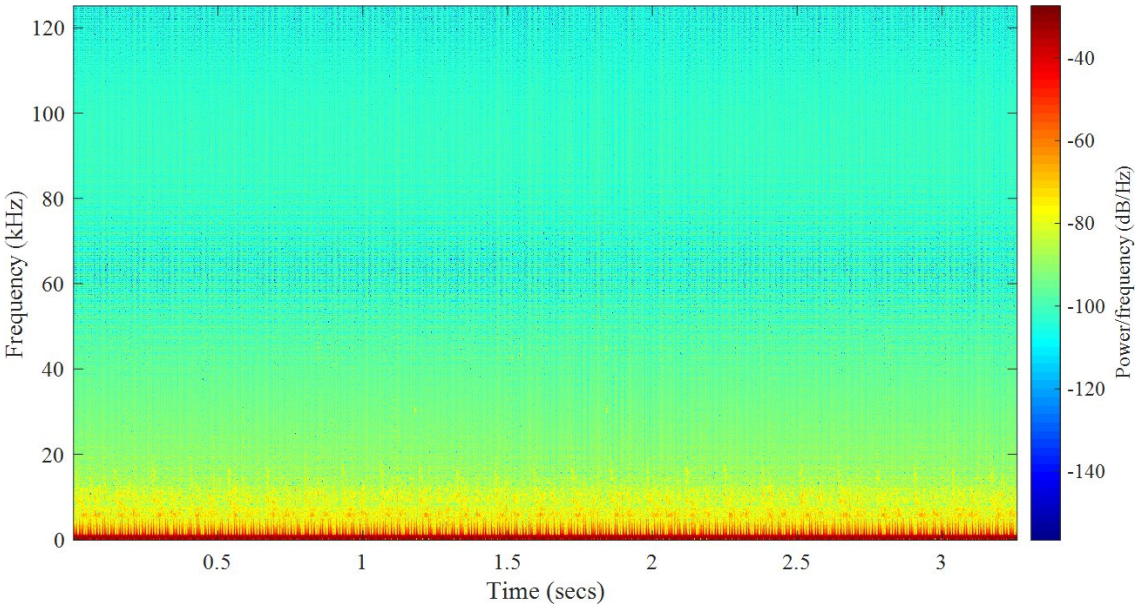

Fig. 35. Θ_2 orientation, baseline signal without the deterrent.

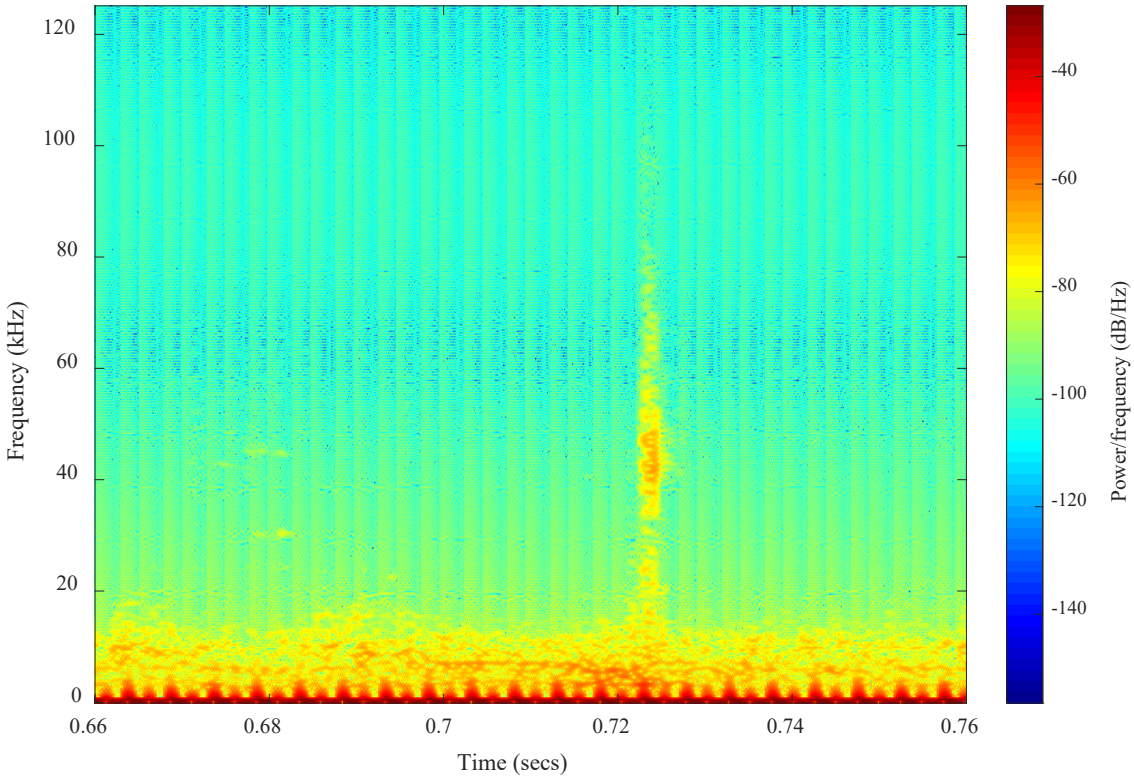

Fig. 36. Example of an ultrasonic burst from the deterrent, recorded from Θ_2 at an average of 150 RPM.

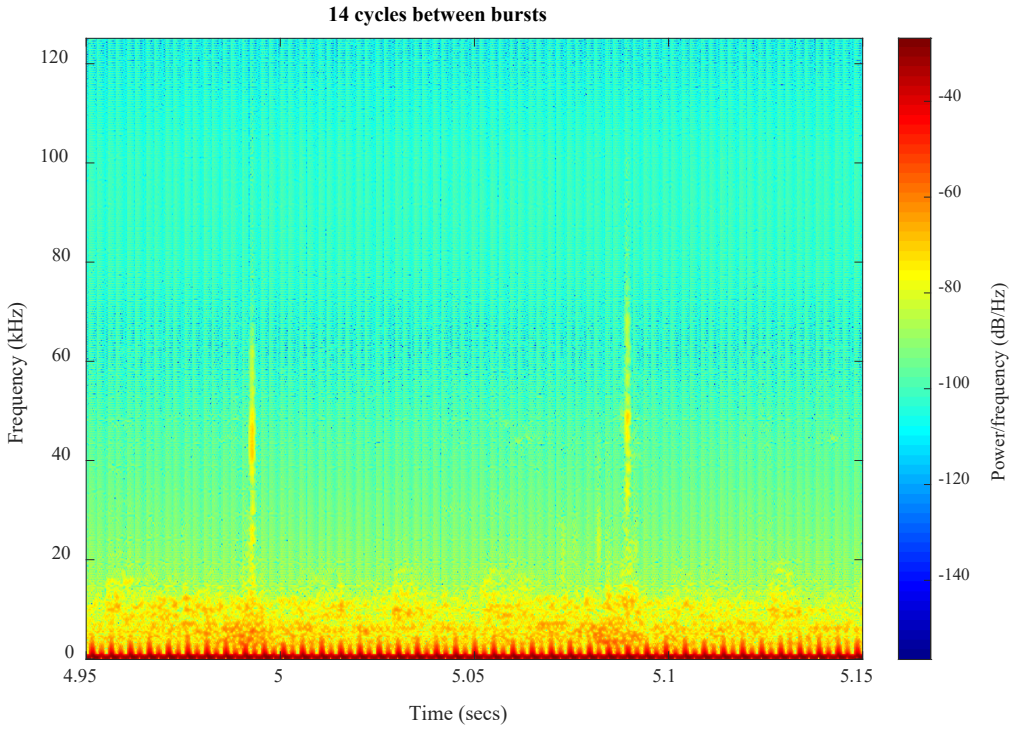

Fig. 37. Example of intermittent emissions as captured from Θ_2, where the pulses arrive between integer multiples of 3 of the low-frequency pulses (we can say it corresponds only to the blade with the deterrent). The rotor fluctuated within 150 ±10 RPM.

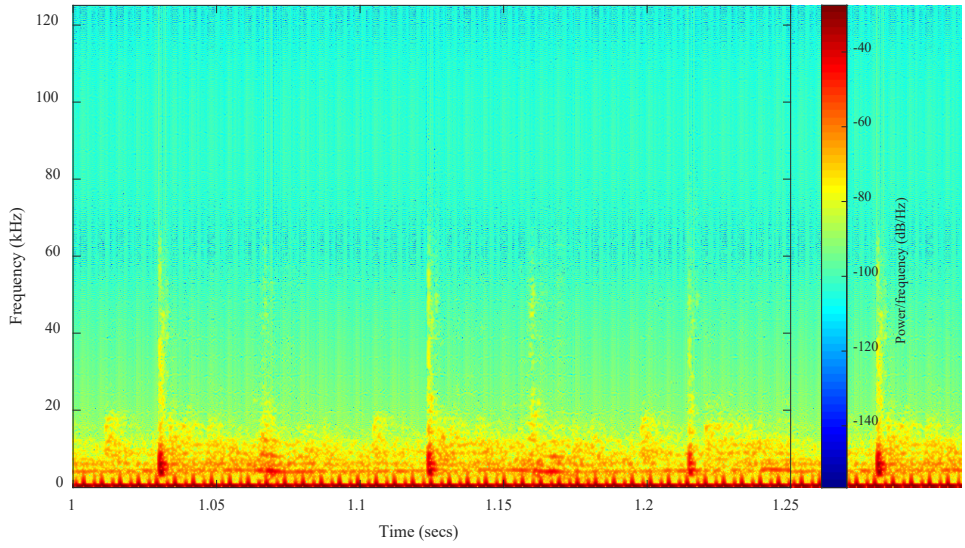

Fig. 38. An axial film response, also at approximately 150 ±10 rotor RPM. Here pulses occur more often compared to the in-plane alignment, which agrees with prior lab testing whereby the in-plane system is less sensitive to flow quality.

Task 6: Define operating variables under which the whistles will need to be able to perform.

Milestone 6.0 - Define operating variables (e.g., wind speeds anticipated at various locations on the rotor, boundary layer conditions) under which whistles will need to perform, and how whistle design will be modified to accommodate.

Deliverable 5 – Produce a report that defines the operating variables under which the whistles will need to perform and how the whistles will need to be modified to functions under these conditions.

DELIVERABLE 5: FLOW CONDITIONS ABOUT A TURBINE BLADE

TASK SUMMARY

In the course of designating the desired flow velocity to actuate our bat deterrent device, we investigated the flow conditions about a rotating wind turbine blade. The current device performance is primarily dependent on the velocity of the incoming flow, leading us to focus on the nature of flow separation along a turbine blade. However, as actual deployed wind turbine blades have proprietary geometries, full-scale deployment of the deterrent will require close collaboration with the blade manufacturers. Such collaboration would permit the design of flow concentrators custom-built for their specific placement along the length of the blade.

Relative velocity due to rotational movement

This deterrent is based on effectively generating ultrasound via mechanical means at wind speeds that bats usually fly under (usually below 5 m/s). However, by being placed on the surface of the turbine blade, there is an additional component to the flow velocity due to rotation. This component scales with both the local length along the blade, as well as the rotational velocity. Though it depends on the specific turbine, the total local flow velocity along the turbine blade is thus several times greater than the freestream velocity. This is known as the tip-speed ratio (TSR). Modern control systems can fine-tune the TSR response to changes in incoming wind and other environmental variables, and an example can be seen in Figure 39 based on the NREL 5 MW turbine. As the current deterrent is capable of operating in the 20-65 m/s range, one can see that the local velocity for a reference turbine near cut-in wind speeds is on an appropriate magnitude for the deterrent. This edge-wise velocity distribution is only one aspect of the flow profile however. The chord-wise flow profile is considerably more complex and equally important to ensure the deterrent is not placed in a region of flow separation.

Accelerating the incoming flow

To design a deterrent agnostic of global flow conditions requires either accelerating or decelerating the incoming velocity to the 20-65 m/s range where the device operates. To this end, computational fluid-dynamic simulations were run within ANSYS Fluent for a concentrator to drive the deterrent response. The flow was modeled with a transient Reynolds-Stress Model, thus accounting for both local turbulence as well as turbulence in the incoming flow. The goal being a general proof-of-concept for concentrators operating at the sizes required for the deterrent prototype. As seen in Figure 40, an atmospheric 20 m/s flow does enter the device, and experiences an acceleration to 46 m/s. Considering 20 m/s is on the low end of edge-wise flow velocities (Fig. 39), this indicates low-speed regions can be accounted for using concentrators. Task 5 is experimentally validating the concentrator performance, for eventually testing the

deterrent on a wind turbine blade. The next topic to consider is flow separation and the chord-wise velocity distribution: factors which could negate the local edgewise flow condition.

Computing the flow velocity

Experimentally, it is impossible to accurately record flow velocity offset from the blade surface. The instrumentation used to measure flow velocity, such as pitot tubes or laser Doppler velocimetry (LDV), would themselves interfere with the flow. However, there has been select full-scale studies which recorded the pressure coefficients along the blade surface of a full-scale turbine. The NREL Phase-VI study (Hand et al., 2001) provides such pressure coefficients for the NREL Phase-VI rotor, tested under laboratory conditions in the NASA Ames wind tunnel.

Numerically there has been much recent work applying computational fluid dynamics (CFD) to resolving the flow field about a rotating wind turbine rotor. By comparing the calculated pressure coefficients along the turbine blade to full-scale experimental turbines, the results of the CFD analysis can be validated. This gives confidence in the calculated far-field flow velocity, which is difficult to measure. The computational study used in the present work (Song and Perot, 2015) validated their results with the same NREL Phase-VI rotor (Hand et al., 2001), and found good agreement with the experimental pressure coefficients and rotor torque for incoming flow velocities of 10 m/s. Typically, these studies are focused on either the far-wake of the rotor, or the pressure directly on the blade surface. The flow profile near the blade is rarely reported, and not to the degree of resolution desired for the present work. Thus, we collaborated with J.B. Perot at the University of Massachusetts Amherst to create additional post-processed results of their published work (Song and Perot, 2015), with a focus on the flow region within 5 cm of the wind turbine blade (this encompasses the current design size of the deterrent).

Post-processing the results

The NREL Phase-VI experiments used counterclockwise rotation of the rotor, thus the definitions usually applied to the NREL 5MW orientation are reversed, namely the pressure (upwind relative to freestream) and suction sides (downwind, lifting side) of the blade. Shown in Figure 41 is the velocity contour directly on the blade's pressure surface, given a constant rotor rotation and incoming flow velocity (10 m/s). Here the flow velocity scales directly as the tip-speed ratio would predict, with the magnitude linearly increasing with radial distance. A similar nature is noted for the suction side of the blade, in Figure 42.

In order to create contours on a surface offset from the blade geometry, we created a pseudo mesh to remap the velocity calculations onto. This mesh is the rotor surface coordinates linearly scaled by, in this work, 5%. For example, each infinitesimal 2D section of the blade had their X-Y coordinates increased by 5%, and the velocity was taken at this new location. Though not a uniform offset distance from the blade, this surface envelopes at maximum a region within 5 cm of the blade, an appropriate distance given the current scale of the deterrent. Seen in Figure 43 is the flow velocity for this surface, oriented towards the pressure side of the blade, with Figure 44 showing the suction side. Using a low-range colormap, we can see that flow remains well attached to the pressure side of the blade, which appears as the velocity magnitude increasing approximately linearly along the length of the blade. In comparison, for the suction side flow separates soon after the leading edge along the entire blade length. Interestingly, this manifests as an increase in flow velocity at our 5% offset surface. The air forms a jet which does not interact

with the blade. While initially we were concerned with the influence of flow separation on the suction side of a turbine blade, this result indicates that this region would actually be a more effective place to actuate a bat deterrent, as the jet provides accelerated flow into the whistle.

While these results generally scale with the turbine blade length, precise placement decisions would require collaboration with the blade manufacturers, as blade geometries can vary greatly. Such collaboration would also resolve decisions relating to icing and fouling of the blade. Depending on the specific turbine location, and placement of the device along the chord length, both of these factors can change in impact dramatically. Given the true flow profile though, filters of appropriate density would be applied, and the correlating velocity drop corrected for in the design of the concentrator.

Conclusions

For a full-scale turbine blade, the edgewise velocity distribution is of appropriate magnitude for actuation of the bat deterrent. For locations closer to the root or farther downstream on the chord, early results show favorable performance for flow concentrators. To better characterize the chordwise flow profile, collaboration with CFD researcher Professor J.B. Perot has yielded novel insight into the flow conditions about an NREL Phase-VI rotor, using prior results which were well correlated with full-scale experimental studies. Velocity contours were considered at a surface 5% larger than the geometry of rotor, encompassing a region at maximum 5 cm above the blade surface. The jet formation which accompanies flow separation on the suction side of the blade proved to be unexpectedly well suited for deterrent placement, enabling the capture of an accelerated flow velocity. The pressure side of the blade showed relatively uniform flow, without significant separation, in agreement with the definition of tip-speed ratio. This depth of investigation is possible for research turbines, as their blade geometry is freely available. One can anticipate however that the nature of these flow separation regions depends heavily on the local and neighboring airfoil sections. As the industry moves to longer and more sophisticated blades, airfoil section coordinates are kept as trade secrets. However, given close collaboration with the blade manufacturers, based on flow concentrator calculations for the current device scale it will be possible to appropriately accelerate or decelerate the local flow.

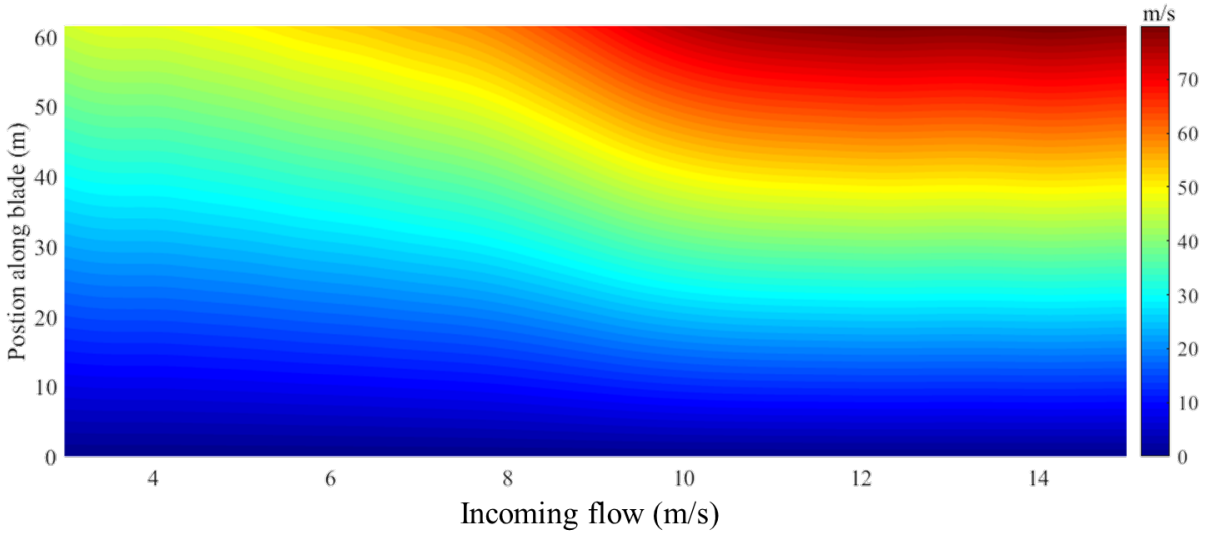

Fig. 39. Local flow velocity along NREL 5 MW reference turbine blade. Derived from Jonkman and National Renewable Energy Laboratory, 2010.

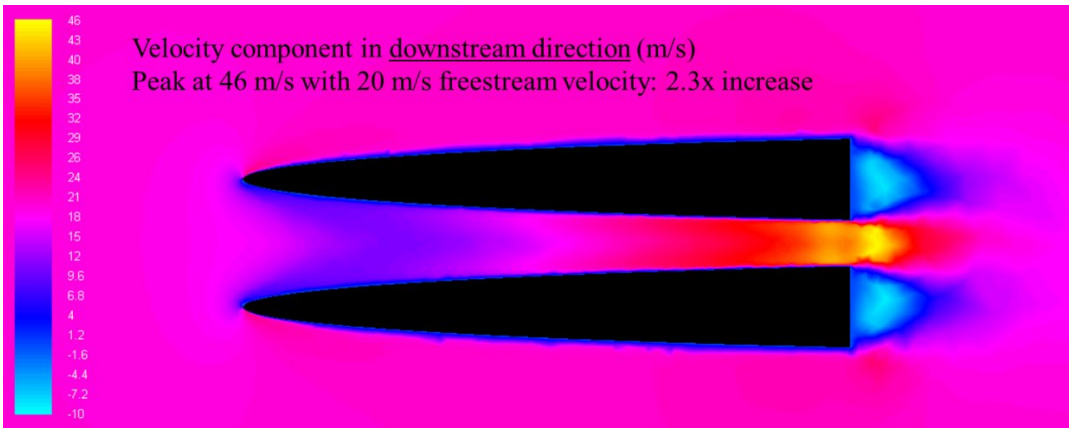

Fig. 40. Concentrator prototype velocity contours, for 20 m/s incoming flow. At the scale of the current prototype, a concentrator could be an effective means of controlling the flow.

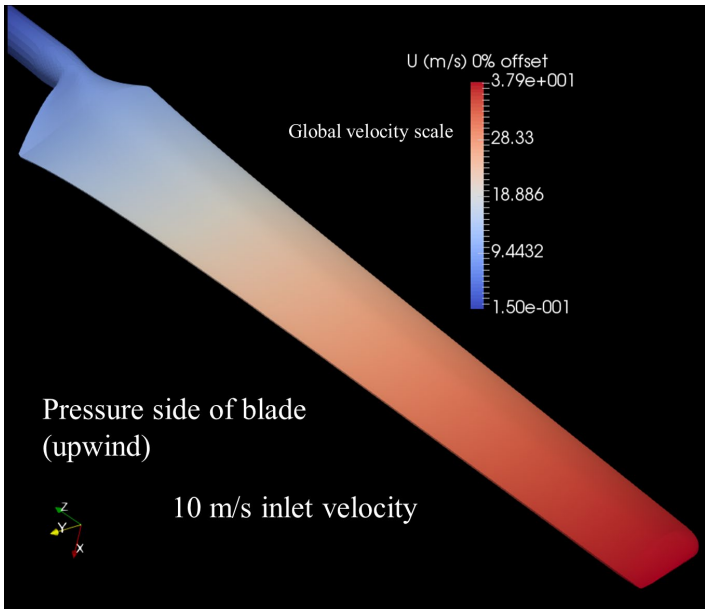

Fig. 41. Blade surface velocity contour of an NREL Phase-VI rotor. The turbine model rotates counterclockwise, hence this is the pressure side of the blade.

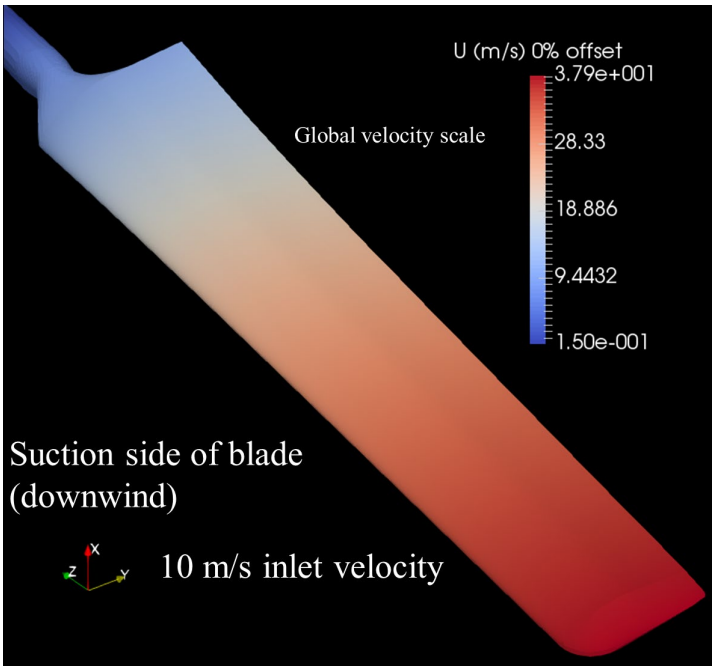

Fig. 42. Blade surface velocity contour of an NREL Phase-VI rotor, suction side.

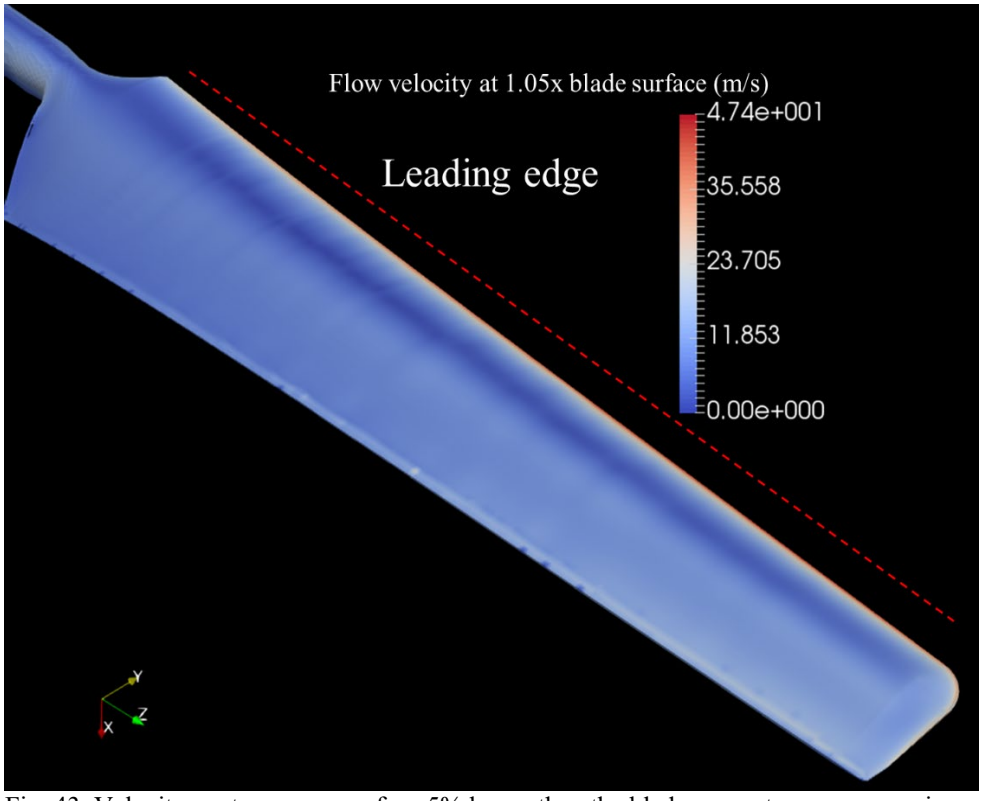

Fig. 43. Velocity contours on a surface 5% larger than the blade geometry, encompassing a region approximately 5 cm from the blade surface at maximum. Facing the upwind side of the blade.

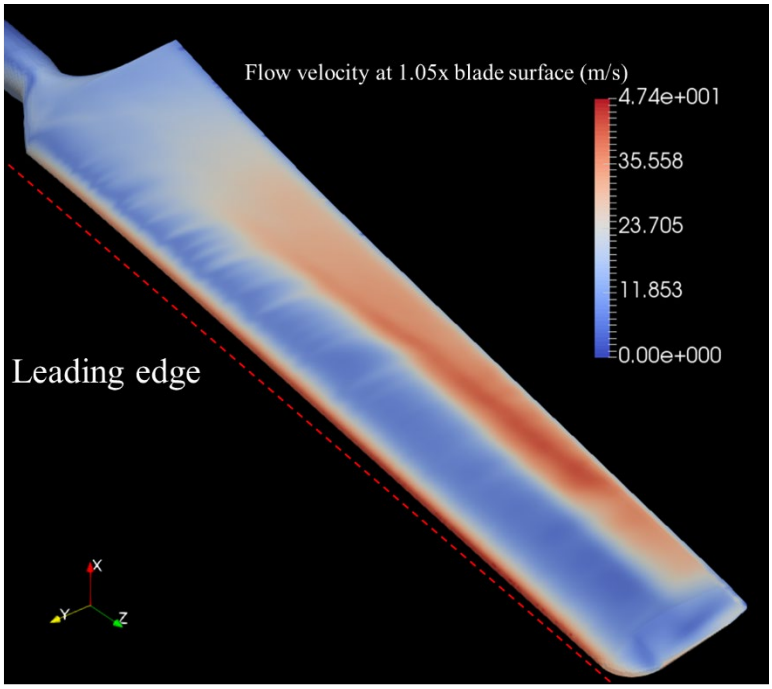

Fig. 44. Velocity contours on a surface 5% larger than the blade geometry, encompassing a region approximately 5 cm from the blade surface at maximum. Facing the downwind side of the blade.

Task 7: Develop a revised biological study design that incorporates the insights from other researchers in the field, and uses only sounds produced from the whistles, rather than generic ultrasonic sounds.

TASK SUMMARY

We completed our first draft of the modified biological study design in April of 2018, received comments, and submitted a second draft in September of 2018. Following discussions with the DOE, and comments from reviewers, we revised the biological study design to include field tests using thermal imaging cameras in 2019. We also requested a No Cost Time Extension to 31 December 2019 to allow us time to complete these new experiments. Below, is the updated biological study design.

DELIVERABLE 6: UPDATED METHODOLOGY FOR BIOLOGICAL STUDY DESIGN

TASK SUMMARY

The behavioral assays have now been amended as requested to add thermal imaging and analyses to the field studies. The field recordings, videography and playback experiments will be combined and executed from the rooftop of a building where bats frequently pass over during the night. The building overlooks a large wooded area where bats are known to regularly fly above the canopy at a height of about 50-60 feet above ground (16-20 meters). Some bats pass overhead at much higher altitudes, but we cannot ensonify that airspace from the rooftop so we will only be analyzing bat passes through the field of view of the two cameras. We will use a combination of thermal imaging video and a microphone array to record and track bats flying

through a designated flight space of approximately 1000 m2 (20 m wide x 50 m deep). At each site we will set up 1) two Axis Q1932-3 thermal imaging cameras positioned at opposite corners of the building rooftop (20 meters apart) and facing outwards over the canopy and oriented at a 45 degree angle (azimuth) towards each other, both focused on the center of a flight space, 2) a four-channel microphone array, and 3) a linear playback array of four speakers spaced 5 meters apart along the edge of the rooftop and oriented to ensonify as much of the target airspace in front of the building and over the tree canopy as possible. Before conducting the experiments, we will empirically measure the spatial dimensions of the stimulus sound field by setting up the sound system at ground level and measuring sound levels with a calibrated microphone positions at multiple positions throughout a 20x50 meter grid. The experimental design will be to perform experiments for 1 hour per evening during the first hour after sunset, switching between playback of acoustic stimuli and silence every ten minutes, and we will alternate which condition to start with each evening. This produces 30 minutes of control (silence) and 30 minutes of playback recordings during the time of night with the most consistent bat activity. The goal will be to obtain combined audio/video recordings over ten nights during March and April of 2019. Video recordings will then be analyzed using the Noldus software suite EthovisionXT and Track3D. Synchronized audio recordings will be analyzed using Matlab and Avisoft Saslab.

The primary aim is to establish whether or not the acoustic stimulus causes a change in bat flight paths. This will be determined from the following measures:

- Counts of bat passes through the flight space, considering trajectory and position relative to speaker array under the two conditions (silence vs whistle-mimic sound at maximum amplitude).
- Determine whether or not any changes in number of bat passes through the air space can be accounted for by bats redirecting their path around the air space.
- If possible, we will analyze any changes in flight path/trajectory while passing through the air space under the two conditions. This will depend on the quality of the computer reconstructions of 2D and 3D flight paths.
- Quantify pulse acoustics or emission patterns under the two conditions that might be related to position or orientation relative to speaker array.

Acoustic Methods

Playback will be presented through four broadband speaker drivers positioned in a linear array 5meters apart and facing the same direction outwards over the tree canopy. While this is somewhat similar to how we envision deploying the deterrent whistles on a turbine blade, the primary goal of this configuration is to ensonify the largest area possible: a larger ensonified space means more bats will be exposed to the stimulus during the trials, which in turn increases the power of the statistical analyses. The playback stimuli are based on spectrograms and Matlab models provided to us by Dan Carlson (Fig. 45). We used Matlab to synthesize the stimuli so that the sounds mimicked as closely as possible the production of the whistle when it is functioning on a turbine. The stimuli are digitized and stored on PC as 10-second long *.wav* files (digital sound files) that are continuously looped for each 10-minute stimulus-ON period. The voltage range of the digital sound files and settings of the analog-to-digital converter and amplifier were optimized to produce a stimulus amplitude of approximately 85 dB SPL from 20-70kHz at the speaker, with minimal harmonic distortions and an empirically determined beam

projection width of approximately 65 degrees (i.e. the stimulus amplitude was attenuated by approximately 10 dB at an angle of 32.5 degrees in any direction, Fig. 46).

To calibrate loudness of the speaker output over the frequency range of the stimulus being presented, we measured the V rms amplitude of the continuous signal at 10 cm and 1m using a calibrated B&K type 4939 ¼" microphone. At 10 cm the stimulus loudness was 85 dB SPL and at 1 m it was 65 dB SPL, consistent with nominal atmospheric attenuation. All of the bats of interest in this project have hearing thresholds within this frequency range at or below 20 dB SPL, meaning that any of these species of bats approaching the speaker on axis should be able to detect the sound more than 100 meters away. However, since in most cases the bats are not approaching the speaker on-axis, the estimated effective range of the stimulus is likely to be significantly less than this. We evaluated an air space extending out to approximately 50 m from the speakers and the thermal imaging data will allow us to assess effects of distance from speaker array on the results.

Acoustic analyses

The acoustic analyses are needed to supplement the video analyses because we need to know if the bats are making any vocal adjustments in response to the stimulus, such as changing pulse acoustics or temporal patterns. The acoustic data might also prove to be useful because it can be used to help reconstruct flight paths, if that proves to be a useful or necessary part of the analyses. We will use Avisoft Saslab Pro for most of the basic ultrasonic analyses. This program is capable of discriminating bat sonar pulses from background noise based on user¬defined threshold criteria, typically amplitude, frequency range, and sound durations. The program also has a multichannel feature that allows extraction of time-of-arrival differences across channels, which can subsequently be used to extract the position of the sound source in space. 3D reconstruction of flight paths is performed in Matlab. The artificial whistle stimulus overlaps with the frequency range of the target bat's pulse emissions, its bandwidth and temporal features are sufficiently different to allow for easy automated discrimination and quantification. Never the less, all recordings are reviewed by eye and evaluated by a technician to confirm automated measurements and extract additional details. All recorded bat passes will be assigned to a species based on spectro-temporal properties of the pulse sequences, although it is predicted that > 90% will be *Tadarida brasiliensis*. If sufficient numbers of other species are detected, those data will be pooled for separate species-specific analyses.

Video Analyses

For video capture we will be using two Axis Q1932-e thermal network cameras with 19 mm lenses (Fig. 47). The horizontal field of view is 32° degrees, and the field of view at 100 meters is 57 meters wide by 43 meters high. The camera resolution is 640 x 480, resulting in a minimum resolution of 11 pixels per meter at that distance. The software requires 8-10 pixels per meter to detect bats, thus we expect to be able to detect and tract bats within a range of less than 100 meters. For video analyses we use a combination of the Axis camera software and the Noldus software suite EthovisionXT. The Axis camera software is best for detection of objects, while the Noldus software allows for 3D video tracking of user-selected objects that fall within the field of view of both cameras. With two cameras we will be able to make accurate assessments of each bat's distance from the speaker array, trajectory and orientation. In some instances, we will be able to use Ethovision's Track3D module to reconstruct flight paths based on the calibrated,

synchronized recordings from two cameras via their audio port, which would provide more details about flight path tortuosity, speed, and distances at which bats change trajectory. However, we were unable to find a representative published example that combined Ethovision software tools with thermal imaging videos, so it is uncertain how well the Ethovision 3D tracking tools will work with this kind of video, but at a minimum we will be able to use this software to calculate distances, positions, and re-create some flight paths. It's anticipated that the software's automated tracking features will work well when bats fly within ~50 meters of the cameras, but passes falling farther out may require manual analyses and flight-path reconstruction. Synchronizing the video and audio recordings will provide more detail about the coupling between locomotor and vocal responses to the playback stimulus, but limits and constraints of the recording and analyses system will remain partly unknown until we set everything up and run the pilot experiments. The default (backup) plan is to manually analyze the video by eye using technicians that are blind to the study conditions (the people analyzing the video will not know when the stimulus is on or off), which would provide at a minimum, reliable numbers of bat passes and address whether changes in bat passes can be accounted for by bats moving further away from the playback speakers. We plan on running pilot experiments in late January or February to calibrate the cameras and playback stimuli, and will have details of the methodology worked out before the spring migration period begins in late March. These pilot experiments will be done first in a large sports field at ground level (to facilitate sound field measurements) and then also at the test site on top of the building. If we run experiments two nights per week (weather permitting) we should be able to collect all the raw data by the end of April and provide preliminary results and analyses by the end of May.

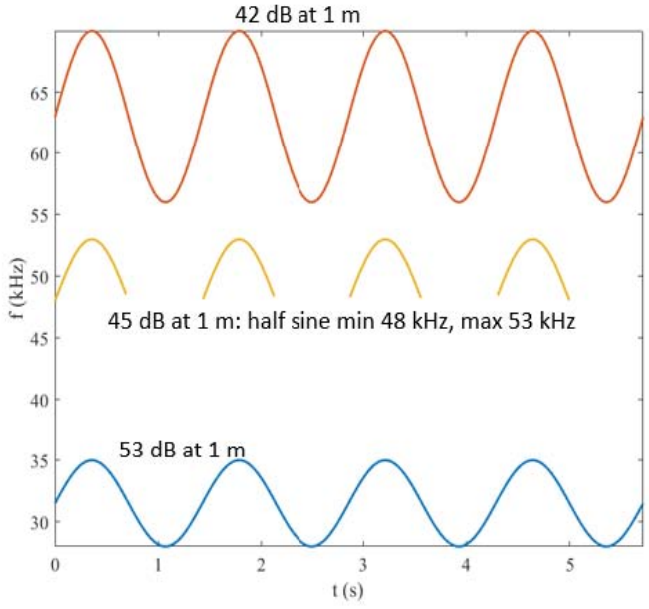


```
NF=0.7;
tt=linspace(0,4./NF,200);

y1=(35-28)./2*sin(2*pi*NF.*tt)+mean([35,28]);
y2=(70-56)./2*sin(2*pi*NF.*tt)+mean([70,56]);

y3=(53-48)*sin(2*pi*NF.*tt);

y3(y3<0)=NaN;

y3=y3+48;
```

Fig. 45.: Acoustic model of stimulus mimicking the sound produced by the whistle.

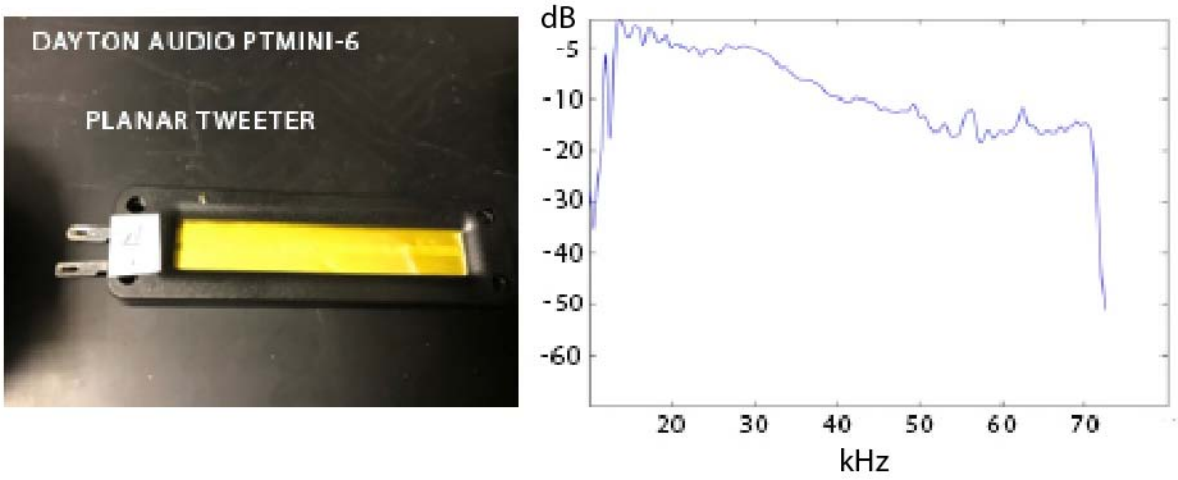

Fig. 46. Frequency response characteristics of the Dayton Audio PTMini-6 Planar Tweeter. In the power spectrum (right) amplitudes are provided relative to maximum output (94dB SPL). Maximum output is 85 dB SPL (0 on the graph above). We can use a calibration curve to flatten the output based on the response profile or adjust the relative amplitudes at different frequencies to mimic the estimated output of the whistle.

Fig. 47. Axis Q1932-E thermal imaging camera to be used in this project. Photo on the right illustrates the approximate field of view and resolution capacity of this model camera (from manufacturer's website).

LITERATURE CITED

Alipour, F, S Jaiswal and S Vigmostad. 2011. Vocal fold elasticity in the pig, sheep, and cow larynges. *Journal of Voice* 25(2): 130-136.

Arnold, B, and G Wilkinson. 2011. Individual specific contact calls of pallid bats (*Antrozous pallidus*) attract conspecifics at roosting sites. *Behavioral Ecology and Sociobiology* 65(8): 1581-1593.

Chanaud, R. 1970. Aerodynamic whistles. *Scientific American* 222: 40-47.

Cveticanin, L. 2012. Review on mathematical and mechanical models of the vocal cord. *Journal of Applied Mathematics* 2012.

Durrant, G. 1988. Laryngeal control of the duration and frequency of emitted sonar pulses in the echolocating bat, *Eptesicus fuscus*. PhD Thesis: Indiana University.

Elemans, C, A Mead, L Jakobsen and J Ratcliffe. 2011. Superfast muscles set maximum call rate in echolocating bats. *Science* 333(6051): 1885-1888.

Fitch, W. 2006. Production of vocalizations in mammals. *Visual Communication* 3(2006): 145.

Hand, M., Simms, D., Fingersh, L.J., Jager, D., Larwood, S., Cotrell, J., Schreck, S. 2001. Unsteady aerodynamics experiment Phase VI: wind tunnel test configurations and available data campaigns.

Harrison, D. 1995. *The anatomy and physiology of the mammalian larynx*. Cambridge University Press.

Hedlund, J, P Curtis, G Curtis, and A Williams. 2004. Methods to reduce traffic crashes involving deer: what works and what does not. *Traffic Injury Prevention* 5(2): 122-131.

Hirano, M. 1974. Morphological structure of the vocal cord as a vibrator and its variations. *Folia phoniatrica et logopaedica*, 26(2): 89-94.

Hirano, M, and Y Kakita. 1985. Cover-body theory of vocal fold vibration. *Speech science: Recent advances*, 1-46.

Hutchins, D, H Jones, and P Vermeulen. 1983. The modulated ultrasonic whistle as an acoustic source for modeling. *The Journal of the Acoustical Society of America* 73(1): 110-115.

Jonkman, J, and the National Renewable Energy Laboratory (U.S.). 2009. Definition of a 5-MW reference wind turbine for offshore system development. Golde, CO: National Renewable Energy Laboratory.

Jonkman, J., National Renewable Energy Laboratory, 2010. Definition of the floating system for phase IV of OC3.

Kobayasi, K, S Hage, S Berquist, J Feng, S Zhang, and W Metzner. 2012. Behavioural and neurobiological implications of linear and non-linear features in larynx phonations of horseshoe bats. *Nature Communications* 3:1184.

Lucero, J. 1995. The minimum lung pressure to sustain vocal fold oscillation. *The Journal of the Acoustical Society of America* 98(2): 779-784.

Mergell, P, H Herzel, T Wittenberg, M Tigges, and U Eysholdt. 1998. Phonation onset: vocal fold modeling and high-speed glottography. *The Journal of the Acoustical Society of America* 104(1): 464-470.

Monsen, R, A Engebretson, and N Vemula. 1978. Indirect assessment of the contribution of subglottal air pressure and vocal-fold tension to changes of fundamental frequency in English. *The Journal of the Acoustical Society of America* 64(1): 65-80.

Murray, P, and S Thomson. 2012. Vibratory responses of synthetic, self-oscillating vocal fold models. *The Journal of the Acoustical Society of America* 132(5): 3428-3438.

Paidoussis, M. P. 2014. Fluid-structure interactions: slender structures and axial flow. 2nd Edition. Academic Press, 888 pages.

Pattie, F. 1924. A blower of the galton whistle. *American Journal of Psychology* 35: 308-309.

Riede, T, H Herzel, D Mehwald, W Seidner, E Trumler, G Bohme, and G Tembrock. 2000. Nonlinear phenomena in the natural howling of a dog–wolf mix. *The Journal of the Acoustical Society of America* 108(4): 1435-1442.

Riede, T, and I Titze. 2008. Vocal fold elasticity of the Rocky Mountain elk (Cervus elaphus nelsoni)–producing high fundamental frequency vocalization with a very long vocal fold. *Journal of Experimental Biology* 211(13): 2144-2154.

Riede, T, A York, S Furst, R Müller, and S Seelecke. 2011. Elasticity and stress relaxation of a very small vocal fold. *Journal of Biomechanics* 44(10): 1936-1940.

Roberts, L. 1975a. Evidence for the laryngeal source of ultrasonic and audible cries of rodents. *Journal of Zoology* 175(2): 243-257.

Roberts, L. 1975b. The functional anatomy of the rodent larynx in relation to audible and ultrasonic cry production. *Zoological Journal of the Linnean Society* 56(3): 255-264.

Scheifele, P, D Browning, and L Collins-Scheifele. 2003. Analysis and effectiveness of deer whistles for motor vehicles: frequencies, levels, and animal threshold responses. *Acoustics Research Letters Online* 4(3): 71-76.

Scripture, E, and H Smith. 1894. Experiments on the highest audible tone. *Studies from the Yale Psychological Laboratory* 2.

Shaw, S, S Thomson, C Dromey and S Smith. 2012. Frequency response of synthetic vocal fold models with linear and nonlinear material properties. *Journal of Speech, Language, and Hearing Research* 55(5): 1395-1406.

Sidlof, P, O Doare, O Cadot, and A Chaigne. 2011. Measurement of flow separation in a human vocal folds model. *Experimental Fluids* 51:123-136.

Song, Y, and J.B. Perot. 2015. CFD Simulation of the NREL Phase VI Rotor. *Wind Engineering* 39:229-310.

Story, B, and I. Titze. 1995. Voice simulation with a body-cover model of the vocal folds. *The Journal of the Acoustical Society of America* 97(2): 1249-1260.

Suthers, R, P Narins, W Lin, H Schitzler, A Denziger, C Xu and A Feng. 2006. Voices of the dead: complex nonlinear vocal signals from the larynx of an ultrasonic frog. *Journal of Experimental Biology* 209: 4984-4993.

Suthers, R, and J Fattu. 1973. Mechanisms of sound production by echolocating bats. *American Zoologist* 13(4): 1215-1226.

Titze, I. 1988. The physics of small-amplitude oscillation of the vocal folds. *The Journal of the Acoustical Society of America* 83(4): 1536-1552.

Titze, I and E Hunter. 2004. Normal vibration frequencies of the vocal ligament. *The Journal of the Acoustical Society of America* 115(5): 2264-2269.

Topman, S, and M Sharp. 2004. *U.S. Patent No. 6,698,377*. Washington, DC: U.S.

Zhang, K, T Siegmund, R Chan, and M Fu. 2009. Predictions of fundamental frequency changes during phonation based on a biomechanical model of the vocal fold lamina propria. *Journal of Voice* 23(3): 277-282.